

# We are IntechOpen, the world's leading publisher of Open Access books Built by scientists, for scientists

6,900

Open access books available

186,000

International authors and editors

200M

Downloads

Our authors are among the

154

Countries delivered to

TOP 1%

most cited scientists

12.2%

Contributors from top 500 universities



WEB OF SCIENCE™

Selection of our books indexed in the Book Citation Index  
in Web of Science™ Core Collection (BKCI)

Interested in publishing with us?  
Contact [book.department@intechopen.com](mailto:book.department@intechopen.com)

Numbers displayed above are based on latest data collected.  
For more information visit [www.intechopen.com](http://www.intechopen.com)



# Crystallization of Iron-Containing Oxide-Sulphide Melts

Evgeniy Selivanov and Roza Gulyaeva

*Institute of Metallurgy of the Ural Branch of the Russian Academy of Sciences  
Russia*

## 1. Introduction

The processing of the sulphide raw materials (ores, concentrates and mattes) of non-ferrous metallurgy is related to the formation of a large amount of iron containing slags. The initial product of the oxidation of sulphides in real commercial plants is an oxide-sulphide melt, in which decomposition under the action of fluxes is accompanied by matte and slag formation (Selivanov et al., 2009a). The fraction of oxygen in a sulphide melt and the fraction of sulphur in an oxide melt are each controlled by the contents of silicon dioxide and iron oxides in a slag and the contents of non-ferrous metals in a matte. According to modern concepts, the heterogeneity of slags is caused by mechanical matte, magnetite and spinel inclusions, where the spinel inclusions form during oxidation processes (Selivanov et al., 2000; Spira & Themelis, 1969; Tokeda et al., 1983; Vanyukov & Zaitsev, 1969, 1973). The cooling (i.e., the crystallization) of a slag leads to the formation of new oxide and sulphide phases within it. Information on the available forms of the useful components is important for the reduction of metal loss through a slag and for the selection of their re-extraction methods.

A number of works are devoted to the study of the kinds of copper existing in slags. Major results are generalized in the monographs of (Ruddle, 1953; Vanyukov et al., 1988; Vanyukov & Zaitsev, 1969; 1973). Phase equilibria in the systems relevant to copper pyrometallurgy have been discussed mostly for molten states (Elliott, 1976; Kopylov, 2001; Yazawa, 1974). It is considered that the loss of non-ferrous metals through slags is caused by their oxide, sulphide and metal solubility. It was discovered that a part of copper is presented in the crystallized slag by matte mechanical inclusions (Vanyukov & Zaitsev, 1969; 1973). Data on the copper sulphide solubility in a slag was reported by (Mohapatra, 1994; Nagamori, 1974; Vanyukov et al., 1988; Vaysburd, 1996). There is no valid confirmation of the presence of individual copper oxide inclusions or copper silicates and ferrites in a slag. Information on the existence of other metals (Zn, Pb, As, etc.) in a slag needs to be specified more exactly in each separate case. The bulk of the zinc is transferred into the slag during the smelting of sulphide copper-zinc concentrates in the Vanyukov furnace for a rich matte and crude metal (Vanyukov et al., 1988). It is assumed herein that zinc is present in a slag in the form of an oxide. Some questions concerning the constituent phases of crystallization during the rapid cooling of a non-ferrous metallurgy slag are partially disclosed by (Cardona et al., 2011). However, no task-oriented studies devoted to

the estimation of the cooling rate's effect on the formation of phases and the presence of different kinds of non-ferrous metals in a non-ferrous metallurgy slag have been found.

The goal of this work is to study phase composition and the kinds of metals present in the slag samples of copper-zinc concentrates of pyrometallurgical processing and the nickel oxide ores of smelting. The main task of the study lies in the estimation of the cooling rate and iron's oxidation level's influence on the phase composition, structure, thermal properties and forms of non-ferrous metals extant in the crystallized oxide-sulphide systems  $\text{FeO}_x\text{-SiO}_2\text{-FeS-Cu}_2\text{O-ZnO}$  and  $\text{SiO}_2\text{-FeO}_x\text{-MgO-CaO-NiO-FeS}$ .

## 2. Methods of investigation

The chemical analysis accuracy resolution is 0.1% for the elements' content in the slag samples over 1% (Fe, S, Zn, SiO, CaO,  $\text{Al}_2\text{O}_3$ ). It is equal to 0.02% when the elements concentration in the slag is less than 1% (Cu, Sb, Pb, As). The phase composition of the samples has been determined by using an X-ray diffractometer (Cu- $K_\alpha$  - radiation). The temperatures and heats of the phase transformations are determined by means of differential-scanning calorimetry with a Netzsch STA 449 C Jupiter thermo-analyser with a heating rate of 20 °C/min in an argon flow. The determination of phase element composition is performed with a JSM-59000LV raster electronic microscope (ESM) and an Oxford INCA Energy 200 dispersion X-ray spectrometer (EDX). The results of the X-ray spectrum microanalysis have (EPMA) a relative error of 2% where the content of the elements is greater than 10%. The relative error is close to 5% at concentrations of elements are from 1% to 10%. This relative error is 10% than concentrations of elements are less 1%. The microstructure of the samples is studied by an Olympus optical microscope using the Simagic application program.

The analysis of the gases evolving in the heating of materials was carried out by a QMS 403C Aëolos mass - a spectrometer connected with the thermo analyser. To perform the thermodynamic simulation (TDS) of the equilibrium phases during the cooling of working bodies whose compositions corresponded to the initial slag samples, we used the HSC 5.1 Chemistry (Outokumpu) software package based on the minimization of the Gibbs energy and variational thermodynamics principles (HSC Chemistry, 2002; Moiseev & Vyatkin, 1999).

The initial slags were put in  $\text{Al}_2\text{O}_3$  crucibles and melted (1300 °C) in a resistance furnace with an electrographite heater for the investigation of the cooling rate's influence on the crystallization of melts. The direct cooling of the slag was carried out in a furnace and it provided for a decrease of the temperature rate up to crystallization (solidus) at about 0.3 °C/s; in the air after removing the crucible from the furnace - 1.7 °C/s; by means of the pouring of the melt from a crucible into a water basin - 900 °C/s. With the water granulation of the slags, we fabricated particles with an average size of 1.5–2.0 mm. The calculation of the cooling time of these particles was carried out using the expression (Naboichenko et al., 1997):

$$\tau_{\text{cool}} = d_d (c_p \rho_{\text{sl}} / 6 \alpha) \ln[(T_m - T_s)/(T_d - T_s)], \quad (1)$$

where  $\tau_{\text{cool}}$  is the drop solidification time;  $d_d$  is the drop size;  $c_p$  is the heat capacity;  $\rho_{\text{sl}}$  is the melt density;  $\alpha$  is the heat-transfer coefficient of the melt-water system;  $T_m$ ,  $T_d$  and  $T_s$  are the temperatures (K) of the slag melt, drop and vapour, respectively. The granules obtained from the slag were subjected to isothermal annealing in an electric resistance furnace (for 5 and 60 minutes) at temperatures of 750 °C and 1000 °C in an inert atmosphere.

The overall strategy of this investigation is presented schematically (Fig. 1).

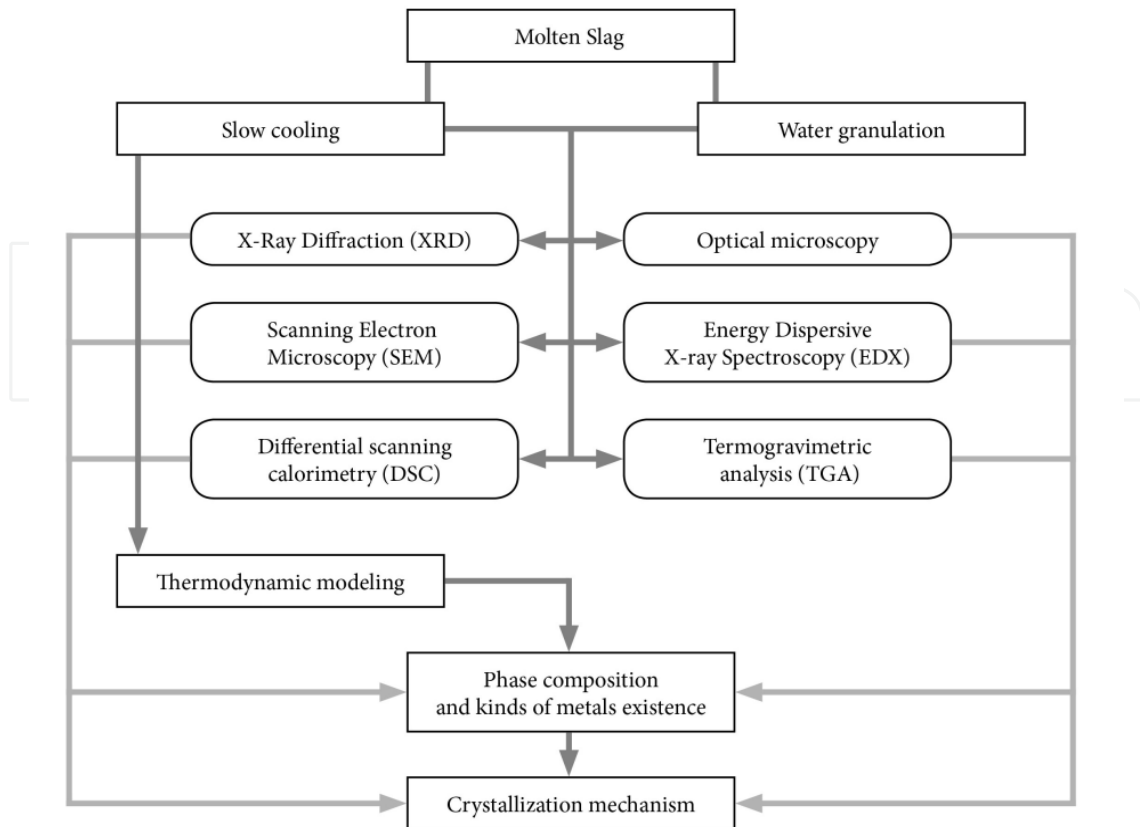


Fig. 1. Overall strategy of this investigation

### 3. Effect of the cooling rate on the structure of slag from the melt of copper-zinc concentrates in a Vanyukov furnace

The autogenous smelting technology of sulphide copper-zinc concentrates in a Vanyukov furnace was developed in “Sredneuralsky Copper Smelter Plant” JSC (Russia, Ural) (Vanyukov & Zaitsev, 1969, 1973; Vanyukov et al., 1988). Concentrates (14 - 16% Cu) are melted for the mattes contents with 45 - 55% copper.

The degree of copper concentration, defined as the ratio of metal content in the matte to its content in the charge, is within the range 3.0 - 4.0. The relatively low quality of the incoming concentrate and the desire to increase the copper content in the matte predetermine the high flow of the oxygen-air mixture and the large amount of slag which is produced. The slag contains iron oxide (III) in the form of magnetite, which largely determines the matte-slag emulsion delamination.

A large number of studies (Jalkann, 1991; Rüffler & Dávalos, 1998; Selivanov et al., 2000, 2004; Vanyukov & Zaitsev, 1969, 1973) have been devoted to the evaluation of slag structure and the metal forms of these of non-ferrous metals are presented in the literature. However, a common law for such complex systems as metallurgical slags does not allow us to extrapolate the known data on the studied samples because new objects require additional study.

The object of the research is the slag from the melting of copper-zinc concentrates in a Vanyukov furnace which contains, %: 40.5 Fe, 2.4 S, 0.8 Cu, 3.9 Zn, 32.1 SiO<sub>2</sub>, 2.8 CaO, 0.8 MgO, 2.6 Al<sub>2</sub>O<sub>3</sub>, 0.1 Sb, 0.5 Pb, 0.1 As (Selivanov et al., 2009b, 2010).

A slag sample is taken from the furnace slag siphon at its overflow into the drain trough. The slag was in contact with a matte containing, %: 44.9 Cu, 23.8 Fe, 2.3 Zn, 22.8 S, 0.1 Sb, 2.0 Pb, until its discharge.

Reflexes which correspond to  $(\text{Fe}_2\text{SiO}_4)$  fayalite,  $(\text{Fe}_3\text{O}_4)$  magnetite and zinc sulphide (sphalerite) are identified in the initial slag through X-ray analysis (Fig. 2). The melting of the slag followed by its cooling reduces the intensity of the X-ray reflexes of the identified phases. Amorphization (glass formation) is reached throughout the mass of the sample when the cooling rate of the slag is equal to  $900\text{ }^\circ\text{C/s}$ .

Thermograms (Selivanov et al., 2009) of the samples (Fig. 3) allow us to estimate the melting and crystallization temperatures of the samples. Two endothermic effects are observed with the heating of the initial slag, which is begun at  $972\text{ }^\circ\text{C}$  and  $1067\text{ }^\circ\text{C}$ .

The first of these characterizes the melting of the eutectic and the second of the entire mass of the slag. The temperature of initial crystallization is equal to  $1021\text{ }^\circ\text{C}$ . According to the mass spectrometry data an evolution of a certain amount of  $\text{SO}_2$  occurred under the sample's heating (from  $300\text{ }^\circ\text{C}$  –  $400\text{ }^\circ\text{C}$ ). This evolution is caused by interaction of sulphides with iron oxides of higher valence. Slag mass loss does not exceed 1.0% with heating up to  $1200\text{ }^\circ\text{C}$ . The view of the sample thermogram crystallized at  $0.3\text{ }^\circ\text{C/s}$  is essentially identical to the results obtained for the original slag.

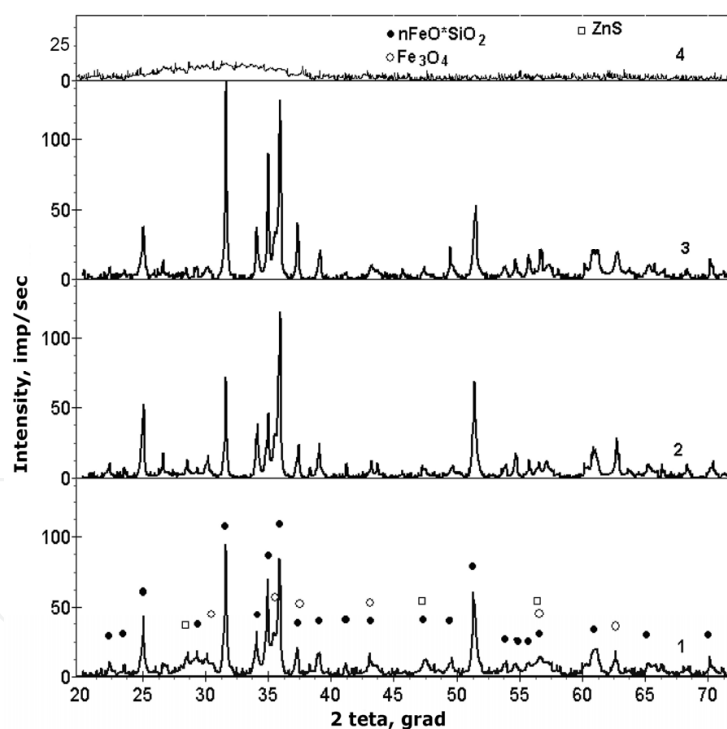


Fig. 2. Diffractograms of the initial (1) slag of melting of copper-zinc concentrates and samples obtained after their melting and cooling rates: 0.3 (2), 1.7 (3),  $900\text{ }^\circ\text{C/s}$  (4).

We may note the proximity of the starting temperatures of the thermal effects associated with melting ( $1062\text{ }^\circ\text{C}$ ) and melt crystallization ( $1045\text{ }^\circ\text{C}$ ). The appearance of the effect on the DSC curve is characterized for a sample cooled at a rate of  $900\text{ }^\circ\text{C/s}$  (Fig. 3). The effect starts from  $507\text{ }^\circ\text{C}$  ( $T_{\text{ons}}$ ) and its middle is at  $533\text{ }^\circ\text{C}$  ( $T_g$ ), which is connected with a second-order phase transition and the resulting process of slag devitrification (Mazurin, 1986) for the

sample cooled at 900 °C/s (Fig. 3). Two exothermal heating effects are revealed on further heating with the onset/maximum at 541/577 °C and 628/644 °C. Apparently, the “cold” crystallization of the slag – the ordering of its structure – takes place at these temperatures and the presence of a doublet of peaks is caused by its two phases.

Devitrification observed on heating the sample containing glass and further “cold” crystallization is connected with the formation of magnetite (exothermal effect) and the isolation of crystals of the iron-silicate phase with a slightly lower (in comparison with glass) quantity of iron oxide:

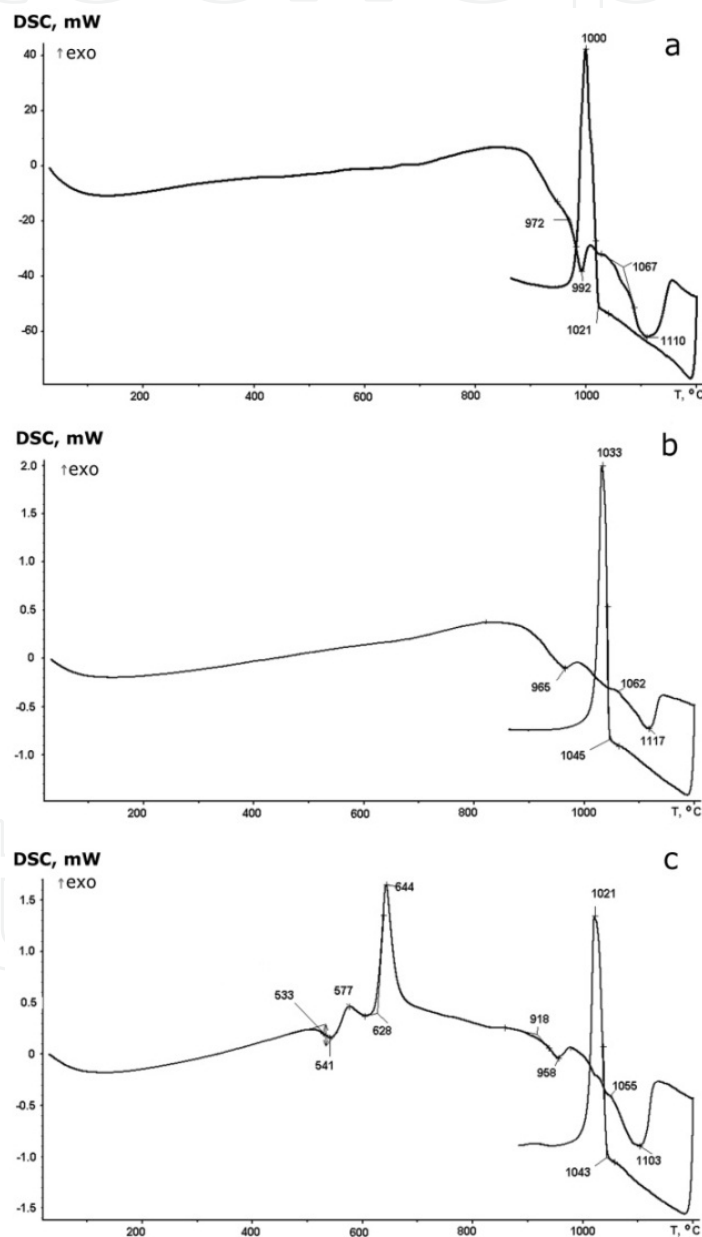


Fig. 3. Thermograms (20 °C/min, argon): of initial slag (a) from the melt of copper-zinc concentrates and the samples obtained after its melting and cooling at the rates of : 0.3 (b) и 900 °C/s (c)

The endothermic effects which started at 918 and 1055 °C point to the melting of the phase components of the slag. The temperature of the initiation of crystallization melting is 1043 °C which agrees with the temperature determined for the sample cooled at a rate of 0.3 °C/s. The temperature values and the change of heat capacity at devitrification ( $\Delta c_p$ ) calculated from the experimental data and from the heat values of the 'cold' ( $L_{c.cr.}$ ) and high ( $L_{h.cr.}$ ) temperature crystallization of the hardened sample of slag are given in table 1. According to the data obtained, the heating of high-iron vitreous slag completely transforms it from an amorphous state to a crystalline state. The heat of slag melting is 165 J/g (Selivanov et al., 2009b).

Devitrification			$L_{c.cr.}$ , J/g		$L_{m.}$ , J/g		$L_{h.cr.}$ , J/g
$T_{ons.}$ , °C	$T_g$ , °C	$\Delta c_p$ , J/(g·K)	1 peak	2 peak	1 peak	2 peak	
507	533	0.756	15	98	13	152	164

Table 1. The values of heat effect enthalpies of slags from a melt of copper-zinc concentrates at samples cooled at a rate of 900 °C/s.

The microstructure (Fig. 4) of the initial slag is represented by iron-silicates, magnetite and matte particles. Magnetite has been formed as fine-dispersed branchy dendrites. The isolated coarse matte particles are mechanically carried out together with the slag, which reach a size of up to 150  $\mu\text{m}$ . The silicate constituent of the slag has small sulphide patches, which reach a size of 1.0-2.0  $\mu\text{m}$ ; they are concentrated along the boundaries of large iron-silicate aggregates. According to the X-ray spectral microanalysis data, the iron-silicate phase (Table 2) is heterogeneous, both in the main elements (silicon and iron) and the impurities dissolved in it. The calculated composition of the iron-silicates ranges from  $\text{Fe}_2\text{Si}_3\text{O}_8$  to  $\text{Fe}_3\text{Si}_2\text{O}_7$ . With the elevation of the Fe/Si proportion in the iron-silicate phases, the content of calcium, sulphur, lead and zinc oxides in them decreases:

Fe	Ca	S	Pb	Zn	
$\text{Fe}_3\text{Si}_2\text{O}_7$	43.4	0.5	0.1	-	3.2
$\text{FeSiO}_3$	34.5	1.7	0.8	0.3	3.6
$\text{Fe}_2\text{Si}_3\text{O}_8$	22.1	7.9	1.6	0.6	4.4

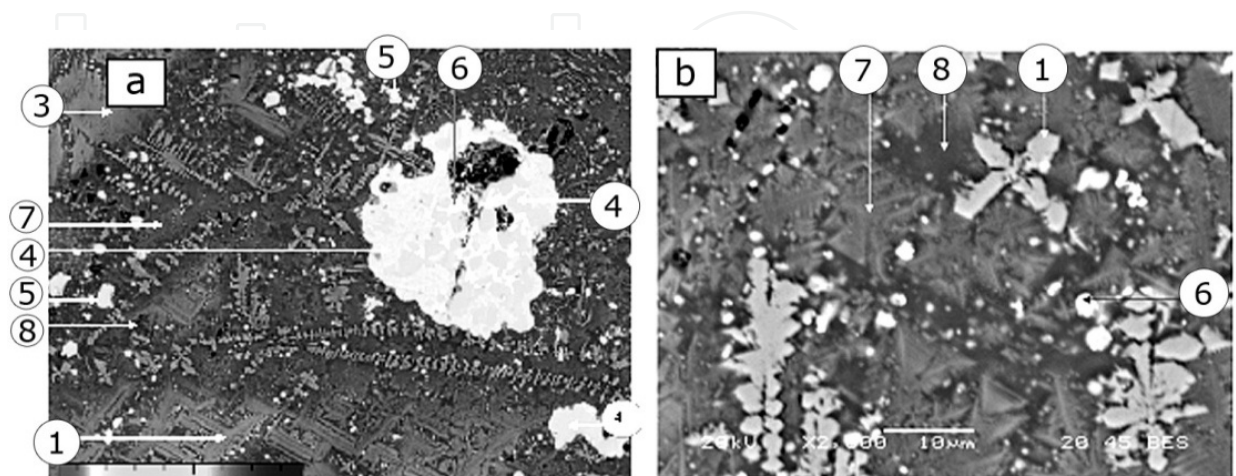


Fig. 4. The microstructure of the initial slag taken from smelting of copper-zinc concentrates and the point of local phase probing

The magnetic crystals (60.5 – 61.9% Fe) which are in the plane of the section also contain impurity elements in %: 1.0 Al; 2.5 - 3.0 Si; 0.3 - 0.4 Ti; 0.1 Cr; 0.1 Mg; 2.2 Zn and up to 0.2 Cu. The sulphide constituents of the slag are represented by the matte particles (48% Cu) with inclusions of zinc and lead sulphides. Solid solutions on the base of a ZnS-FeS system have a composition within the limits of  $Zn_{0.24}Fe_{0.76}S$  to  $Zn_{0.45}Fe_{0.55}S$  and, apart from the primary elements, contain 4.7-6.1% Cu and up to 0.5% Pb.

The iron-silicate phases which have different compositions in which magnetite and sulphides are found (Fig. 5) also constitute the base of the sample cooled at the rate of 0.3 °C/s. In comparison with the initial slag, the enlargement of iron, magnetite and sulphide silicate crystals has been marked. The main area of the matte is occupied by the conglomerates of coarse crystals of the iron-silicate phase, having a composition close to  $Fe_3Si_2O_7$ , and the spaces among them are filled up by  $Fe_2Si_3O_8$  with small dendrites of  $FeSiO_3$ . As well as for the initial slag, the content of the impurity elements correlates with the iron content in the silicate:

Fe	Ca	S	Pb	Zn	Mg	
$Fe_3Si_2O_7...$	44.8	0.3	-	-	2.8	1.1
$FeSiO_3$	36.9	1.7	0.3	-	3.2	0.2
$Fe_2Si_3O_8$	23.5	4.3	1.0	0.4	4.0	-

№	Content, mas. %											Composition
	Mg	Al	Si	S	Ca	Ti	Fe	Cu	Zn	Pb	O	
1	0.1	1.0	2.5-3.0	0.1	0.3	0.3-0.4	60.5-61.9	0.2	2.2	-	31.5-31.7	$Fe_3O_4$
2	0.9-1.0	0.3-0.4	14.0-14.7	0.1	0.4-0.5	-	42.8-44.0	-	3.1-3.3	-	36.8-37.3	$Fe_3Si_2O_7$
3	-	-	0.2	27.1	-	-	20.6	48.8	3.0	-	-	$Cu_{2.1}FeS_{2.3}$ (matte)
4	-	-	0.2-0.3	32.4-32.5	0.1	-	38.2-38.6	25.1-26.0	2.7-3.2	0.5	-	$CuFe_{1.6}S_{2.4}$
5	-	-	0.5-1.4	33.2-32.6	0.2-0.5	-	43.0-30.8	6.1-4.7	16.9-29.8	0.5	-	$Zn_{0.24}Fe_{0.76}S$ $Zn_{0.45}Fe_{0.55}S$
6	-	-	0.2-0.5	20.0-23.3	-	-	12.7-19.5	19.1-23.8	0-4.8	33.3-41.9	-	(Pb,Cu,Fe)S
7	0.4	1.2	17.5	0.7-0.9	1.4-1.9	-	33.9-35.0	0.2	3.3-3.9	0.2-0.3	39.1-39.8	$FeSiO_3$
8	0.1	2.0-2.5	19.7	1.5-1.7	7.1-8.7	0.3	21.9-22.2	0.2	4.4	0.5-0.6	40.7-41.0	$Fe_2CaSi_3O_8$

Table 2. EPMA data on the phase composition of the initial slag from the smelting of copper-zinc concentrates (according to Fig. 4)

Matte particles with sizes from 1 to 15-30  $\mu m$  are found mainly between iron-silicate blocks of a  $Fe_3Si_2O_7$  composition. Matte decomposition into sulphides (bornite, sphalerite, galenite) occurs at cooling and their compositions - according to the analysis data - fluctuate widely (Table 3). More easily melted is lead containing a sulphide alloy from the margin along the

surfaces of the matte particles. High-ferrous sphalerite ( $Zn_{0.4}Fe_{0.6}S$ ) has been revealed both as an independent phase of around 2-10  $\mu m$  in size and the inside of matte particles.

Magnetite (60.0-60.4% Fe) takes the form of both geometrical crystals and the form of dendrites arranged between  $Fe_3Si_2O_7$  blocks and in direct contact with  $Fe_2Si_3O_8$ , both as in the initial slag and in the magnetite apart from the iron, which have revealed zinc, silicon and aluminium impurities as well as titanium (0.6%) and chromium (0.1%).

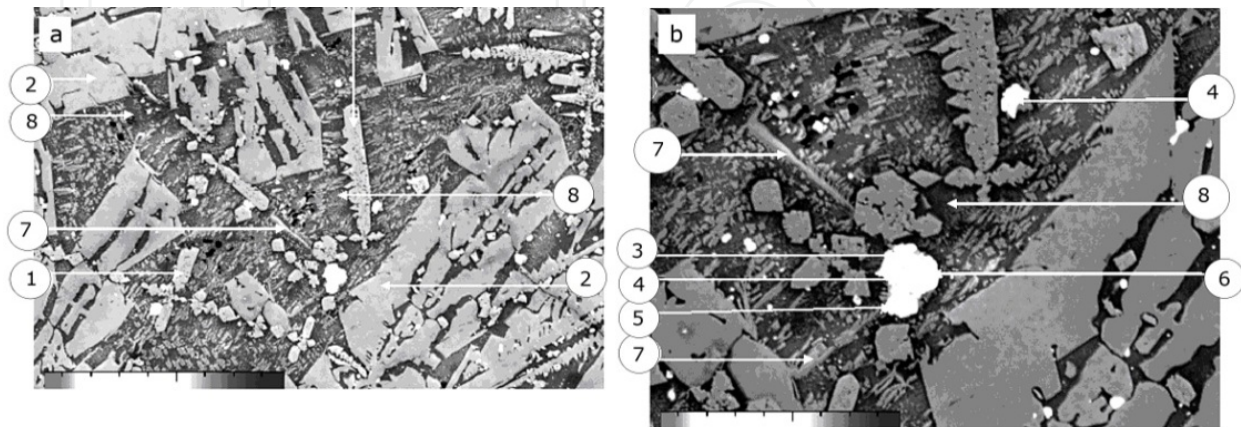


Fig. 5. Microstructure of the slag of copper-zinc concentrates' melting cooled from the melt at the rate of 0.3 °C/sec and the points of local phases' probing: an increase of x200 (a) and x500 (b)

The structure of a slag sample cooled at a rate of 900 °C/s is represented (Fig. 6) by glass and sulphide inclusions (up to 20  $\mu m$ ) with round forms. According to EPMA, the glass contains about 30%  $SiO_2$  and 50%  $FeO_{1+x}$  (Table 4). The sulphide phase (inclusion of more than 15  $\mu m$  in size) is inhomogeneous in its composition - its central part closely corresponds to  $Cu_5FeS_4$ . Lead and zinc sulphides are revealed inside matte particles.

№	Content, mas. %									Composition
	Al	Si	S	Ca	Fe	Cu	Zn	Pb	O	
1	2.5-2.6	1.7-2.0	-	0.2	60.0-60.4	-	2.8	-	31.4-31.6	$Fe_3O_4$
2	-	13.9-14.3	-	0.3	44.3-45.2	-	2.8-2.9	-	36.7-37.0	$Fe_3Si_2O_7$
3	-	0.3	26.7	-	18.9	53.0	0.6	0.8	-	$Cu_5Fe_2S_{4.5}$ (matte)
4	-	0.3-0.5	32.5	0.1	37.8	27.6	1.4	0.6	-	$Cu_2Fe_3S_{4.5}$ (matte)
5	-	0.6	27.8	0.1	35.7	6.1	26.7	3.0	-	$Zn_{0.4}Fe_{0.6}S$
6	-	0.3	18.2	-	13.0	17.0	1.0	50.6	-	$PbS-Cu_2S-FeS$
7	1.1-2.3	16.0-18.1	0.2-0.4	1.1-1.4	34.7-39.0	-	3.0-3.4	-	38.1-39.5	$FeSiO_3$
8	4.0-4.3	20.3-20.6	0.9-1.1	4.2-4.4	23.4-23.6	-	3.8-4.1	0.4	41.4-41.6	$Fe_2Si_3O_8$

Table 3. EPMA data on the composition of slag sample phases after their melting and cooling at a rate of 0.3 °C/s (according to Fig. 5)

The phase close to fayalite ( $Fe_2SiO_4$ ) has not been revealed in any of study samples. All of the complexes of iron-silicate phases that were formed during slag cooling correspond to the

atomic relations of Fe/Si within the limits of 0.7-1.5. Slag cooling at the high (900 °C/s) rate results in the formation of glass with the proportion of Fe/Si equal to about 1.4, without isolating magnetite in a self-dependent phase.

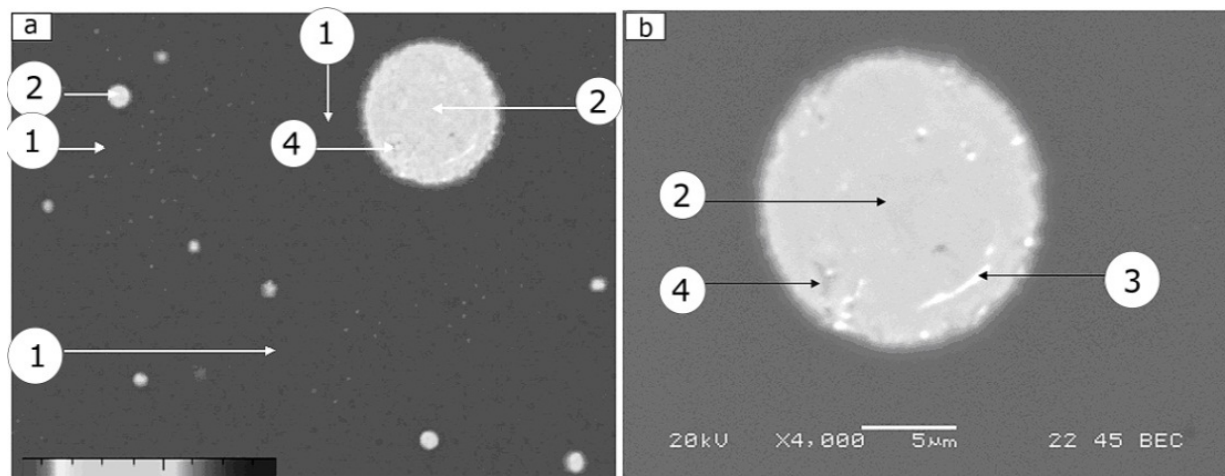


Fig. 6. Microstructure of the slag of copper-zinc concentrates' melting cooled from the melt at the rate of 900 °C/s and EPMA points

№	Content, mas.%										Composition
	Al	Si	S	Fe	Cu	Zn	Pb	O	Mg	Ca	
1	1.8-2.1	13.9-14.0	0.8	38.4-38.9	0.2-0.6	3.7-3.9	0.3-0.4	37.5-37.6	0.4	1.85	Fe <sub>1.4</sub> SiO <sub>3.4</sub> (glass)
2	-	0.3-2.0	21.9-23.7	12.5-14.6	59.6-61.4	0.3-0.6	0.8-1.7	-	-	-	Cu <sub>5</sub> FeS <sub>3.3</sub>
3	-	0.4	23.3	11.6	44.7	16.3	1.7	-	-	-	Cu <sub>5</sub> FeS <sub>4</sub> -(Zn,Fe)S
4	-	0.3	21.1	9.7	57.9	0.3	8.0	-	-	-	Cu <sub>5</sub> FeS <sub>4</sub> -PbS

Table 4. EPMA data on the phase composition of the slag samples cooled from the melt at the rate of 900 °C/s (according to Fig. 6)

Proceeding from the fact that oxide phases with a high content of iron contain a lower quantity of CaO, one can draw a conclusion about the influence of a lime flux on phase formation (Selivanov et al., 2009a). For those slags with a Fe/SiO<sub>2</sub> ratio higher than 1, the increase of calcium oxide will not cause its solution in Fe<sub>3</sub>Si<sub>2</sub>O<sub>7</sub> but rather will favour the decomposition of this compound, which proceeds - in the limiting case - with the formation of calcium silicate and iron oxides. If the Fe/SiO<sub>2</sub> ratio in the slag is less than 1, then the CaO will dissolve in iron-silicate phases (FeSiO<sub>3</sub> and Fe<sub>2</sub>Si<sub>3</sub>O<sub>8</sub>), reducing their melting temperature. One should bear in mind that these points are applied to those oxide melts which do not contain iron oxides of the highest valency. As has been shown in the works of (Okunev & Galimov, 1983; Tokeda et al., 1983), in oxide melts with a high degree of iron oxidation, CaO and Fe<sub>2</sub>O<sub>3</sub> interaction establishes the formation of calcium ferrites.

Slow slag precipitation leads to the concentration of the matte particles among large grains of Fe<sub>3</sub>Si<sub>2</sub>O<sub>7</sub>. On cooling, sulphide phases - the bulk of which is bornite - and crystallize from the matte. This is besides the fact that small crystals of sulphides form in the course of slag

cooling, which can be explained by the peculiarities of the segregation of the oxide-sulphide system and by the change of the sulphides' solubility in iron-silicate melts.

The zinc on slag crystallization is distributed between oxide and sulphide phases. A (Zn,Fe)S independent phase containing 17-38% zinc has been revealed only at low rates of slag cooling. Lead in the slag takes both oxide and sulphide forms. The lead content in the iron-silicate phase increases as the content of silicon dioxide grows in it. Lead forms sulphide phases with 33-51% Pb which precipitate out of the sulphide melt (matte) on cooling (Selivanov et al., 2009b).

Thus, the rate of cooling of the melted slag influences the size and the number of forming phases, which defines the copper, zinc and lead distribution between oxide and sulphide forms. Changing the content of the calcium oxide in the slag and the rate of cooling, one can provide the preparation of the material for the subsequent redistribution of the precious metal's re-extraction. For example, in order to finish the slag by the floatation method (Dovshenko et al., 1997; Korukin et al., 2002; Sarrafi, 2004) it is necessary to form rather large sulphide particles, which is achieved by the familiar processes of reducing the cooling melts rate. The isolated concentrates besides copper will contain other non-ferrous metals, which designates their accumulation and concentration in the semi-products of closed-circuit processing schemes. The calcium oxide content and the rate of slag cooling also influence the composition of iron-silicate forming phases, the properties of which determine the expenditure of energy on slag grinding. The information about the structure of the high-ferrous slag cooled at the high rate allows us to define characteristics of the glassy condition, including the devitrification temperature, heat and temperature, meaning the solid and liquid phases' crystallization of the quenched slag.

Oxide materials are important for pyrometallurgical processes for the production of non-ferrous metals, which are characterized by composition complexity and - apart from iron, silicon, calcium and aluminium oxides - contain the impurity elements Cu, S, Zn, Pb etc. Depending upon the composition and cooling rate from the melted state, the solid samples of oxide systems can be singled out both in crystalline and amorphous states. It is known that in oxide systems containing more than 50% SiO<sub>2</sub> and up to 20% of Fe<sub>2</sub>O<sub>3</sub>, a glassy state is formed even at a low cooling rate (Karamanov & Pelino, 2001). It is shown (Selivanov et al., 2009b, 2010) that all of the complex of iron-silicate phases generated during sample slow cooling corresponds to a molar Fe/Si ratio within the limits of 0.9-1.6. Sample cooling with a high (900 °C/s) rate results in the increase of this ratio by up to 3.4. It should be noted that a decrease of the cooling rate results in the increase of the portion and size of magnetite crystals and sulphide particles.

In connection with the study, the conditions of crystals' formation from amorphous high iron oxides based on FeO<sub>x</sub>-SiO<sub>2</sub>-MeS (Me - Cu, Zn) systems and the determination of the forming phases' composition are of great interest.

The sample of slag from the melt of copper-zinc concentrates in the Vanyukov furnace was melted in the furnace at a temperature of 1250 °C and cooled down using the water granulation method. The cooling rate of the oxide melt calculated from equation 1 is 900 °C/s. The granules obtained are isothermally annealed in the resistance electric furnace (during 5 and 60 min) at a temperature of 750 °C (Gulyaeva et al., 2011).

X-ray analysis results (Selivanov et al., 2009b) have shown that with the cooling of the oxide melt at a rate of about 900 °C/s, an amorphous product is formed (Fig. 2). The reflexes

corresponding to the crystal phase are virtually absent at the diffractogram; however, the diffusion scattering characterizing the availability of a short-range order in the formed glass was observed.

The thermogram received by means of a quenched sample heating is shown in Fig. 3. Based on the data received, the heating of high iron vitrified oxides up to 1230 °C and their cooling at a rate of 20 °C/min results in their transition from an amorphous to a crystalline state. The stability factor of the vitreous state is shown in the following equation (Biswas et al., 2010):

$$\Delta T = T_g - T_{c.cr.} \quad (3)$$

where  $T_g$  and  $T_{c.cr.}$  – devitrification temperatures (533 °C) and the onset of “cold” crystallization (555 °C). For the sample under study, the  $\Delta T$  value amounts to 22 degrees, which points to the non-stability of the amorphous state.

The annealing of sampled granular particles of slag at a temperature of 750 °C does not result in the external change of their forms. The data (Gulyaeva et al., 2011) of the X-ray analysis of amorphous oxide samples after annealing for durations of 5 and 60 min showed that the material heating results in the formation of a crystalline state. In diffractograms (Fig. 7), reflexes of annealed samples typical for fayalite, quartz and magnetite (very weak) were detected. Fayalite reflection ( $d = 2.50 \text{ \AA}$ ) intensity increases from 74 (Fig. 7 a) to 86 pulses/s (Fig. 7 b) with the growth of the annealing duration, whereas magnetite reflection ( $d = 1.48 \text{ \AA}$ ) intensity does not change and is equal to 11 pulses/s.

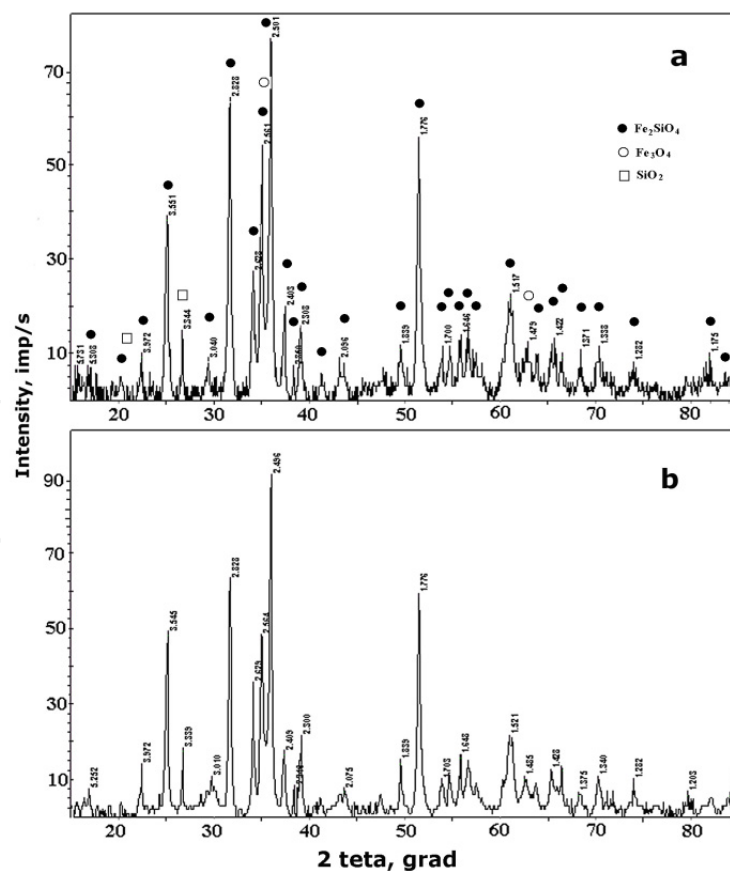


Fig. 7. X-ray spectra of granular slag samples from the melts of copper-zinc concentrates annealed at 750 °C within 5 (a) and 60 min (b)

The microstructure analysis of the samples (Fig. 8) received after annealing showed that initially ( $\tau = 5$  min) single faceted crystals of magnetite are presumably formed. Over the entire area of the metallographic section, a thin grid of crystal is formed with a cell size of 0.3 - 0.5  $\mu\text{m}$ . It should be noted that an increase of the annealing duration ( $\tau = 60$  min) of an amorphous sample results in formation of certain particles of larger dendrites with the axes of the second- and third-order in the area close to the surface. Closer to the particles' border, the dendrites' axes' length decreases, the phases having - in the metallographic section plane - a structure in the form of triangles and stars sized of 5-10  $\mu\text{m}$  form around them. Proceeding from the thermal analysis data (Sycheva & Polyakova, 2004), one can evaluate the viscosity crystallization criterion, which is equal to:

$$\alpha = T_g/T_m \quad (4)$$

where  $T_m$  - temperature of the dissolution of the crystalline phases in the melt (1103  $^{\circ}\text{C}$ ), defining together with the forces of surface tension the capacity of glasses to volume crystallization. The value of  $\alpha$  calculated by this equation reached 0.6, which shows the inclination of the studied oxide glass-to-surface crystallization. The mechanism of the initial formation of crystalline phases is apparently explained by the annealing temperature (750  $^{\circ}\text{C}$ ) which is higher than that of cold crystallization. During the heating of a quenched sample from an oversaturated silicate phase forming the glass diffusion separation of magnetite and the formation of iron-silicate phase crystals, there occurs a little less (compared to glass) iron content through equation 2.

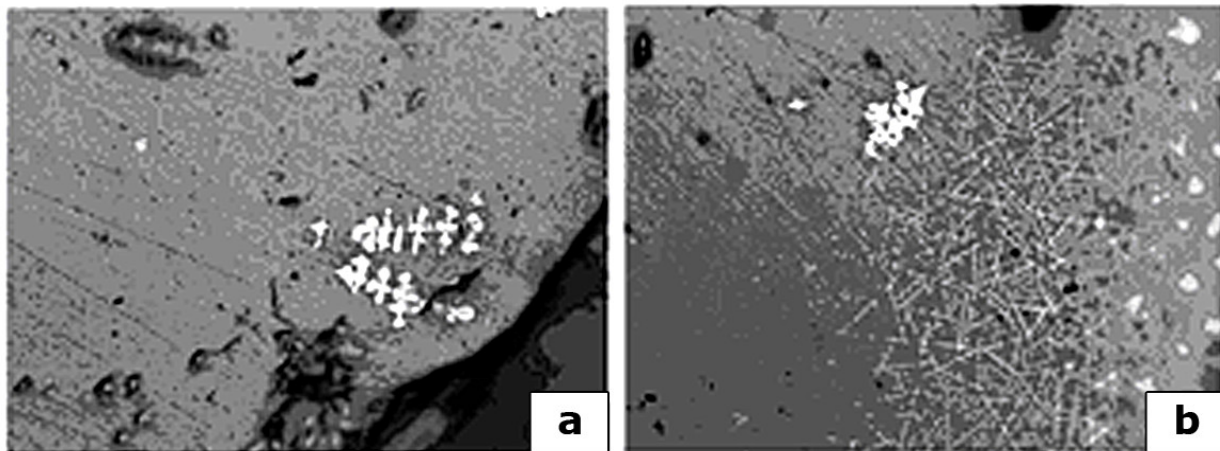


Fig. 8. Microstructure of the slag sample (x500) annealed at 750  $^{\circ}\text{C}$  during 5 (a) and 60 min (b)

The analysis of the sample annealed within 60 min by the X-ray spectral microanalysis of the characteristic radiation of the elements showed that the basis of the dendrite phase is formed by iron oxides while the basis of glass is formed by iron-silicates. The composition of the dendrite phases depending on crystal forms is variable - one of the phases in the form of triangles and stars is richer in iron and close to magnetite in its composition. They contain fewer impurity elements of silicon (0.9%) and calcium (0.2%) (Fig. 9, Table 5). Copper (0.2-0.7%) and zinc (2.7-3.7%) concentrations in magnetite are virtually unconnected with the geometric form of crystals. The silicate phase is close in composition to  $\text{Fe}_{1.36}\text{SiO}_{3.36}$ : the content of copper in it reaches 0.8% and that of zinc reaches 4.1%. The presence of sulphur determines the formation of fine bornite phases of non-spherical forms (1-6  $\mu\text{m}$ ) in the sample and larger chalcosine phases with a size of 15 - 25  $\mu\text{m}$ .

Thus, the granulation of iron-silicate oxide melts containing more than 30% SiO<sub>2</sub> results in the formation of glass. The annealing of the granuled slag of the autogenous smelting of copper-zinc concentrates at 750 °C results in the initial separation of magnetite in the form of geometric crystals from an oversaturated iron-silicate matrix and – furthermore – in the form of a dendrite structure. The diffusion mechanism of magnetite crystals' growth has a superficial character. The composition of the crystallizing phases and the dissolubility of nonferrous metals in them have been established.

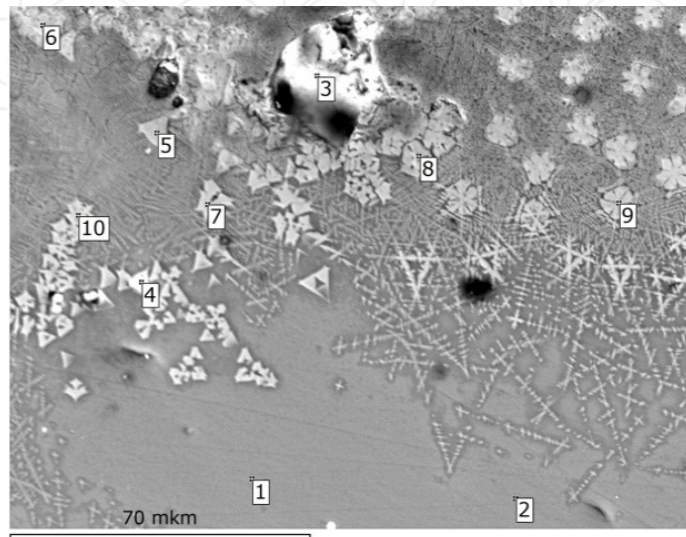


Fig. 9. Microstructure of the sample after annealing at 750 °C within 60 min and EPMA points

№	Content, mass, %					
	Si	Fe	S	Cu	Zn	Al
1	14.9	40.4	0.5	0.8	3.8	2.7
2	14.6	41.1	0.4	0.5	4.1	2.8
3	0.2	3.5	21.5	76.5	-	0.5
4	5.7	26.2	7.9	20.9	2.7	1.7
5	0.9	69.6	-	0.4	2.7	1.9
6	4.1	61.9	0.3	0.6	3.7	2.0
7	4.9	60.7	0.1	0.2	2.6	2.8
8	2.3	64.5	0.1	0.7	3.8	2.2
9	3.1	63.3	-	0.2	3.7	2.7
10	2.4	64.7	-	0.4	3.4	2.7

Table 5. EPMA data on the phase composition of a quenched slag sample annealed at 750 °C during 60 min (Fig. 9)

#### 4. Effect of the cooling rate on the phase composition and structure of copper matter converting slags

As was mentioned (Selivanov et al., 2009a, 2009b), the distinguishing feature of the production process in the “Sredneuralsky Copper Smelter Plant” lies in the fact that mattes containing 45–55% copper recovered upon the smelting of copper-zinc concentrates in the

Vanyukov furnace are converter. Apart from copper and precious metals, the mattes concentrate zinc, lead, arsenic and antimony. During the conversion, a part of these metals passes into a gas phase and dust, and the other part of the metals is redistributed between white matte and slag and then between copper and slag. Thus, the precipitating converter slags have a high content of precious metals, the re-extraction of which increases the coefficient of an integrated approach to the raw materials' use. The choice of the slag processing method is determined based upon the forms of the metals.

A thermodynamic simulation (TDS) was performed for the working body of the following composition, %: 21.0 FeO; 16.0 Fe<sub>2</sub>O<sub>3</sub>; 20.3 SiO<sub>2</sub>; 5.1 ZnO; 11.0 CuO; 2.6 Al<sub>2</sub>O<sub>3</sub>; 2.0 CaO; 1.2 MgO; 2.0 Sb<sub>2</sub>O<sub>3</sub>; 1.2 Pb, 3.1 S. The degree of iron oxidation ( $\alpha$ ) in the working body determined Fe<sup>3+</sup>/Fe<sup>2+</sup> the ratio amounts as 0.4. During the thermodynamic simulation, we used the compounds inherent in the FeO<sub>x</sub>-SiO<sub>2</sub>-FeS-Cu<sub>2</sub>O-ZnO system. The calculations were carried out for the 100 kg working body at a gas phase (nitrogen) volume of 2.24 m<sup>3</sup> over the slag and at a pressure in the system equal to 0.1 MPa.

According to the TDS results, the main components of the equilibrium system which was cooled under equilibrium conditions were: Fe<sub>3</sub>O<sub>4</sub>, Fe<sub>2</sub>SiO<sub>4</sub>, SiO<sub>2</sub>, ZnS, Cu<sub>2</sub>S, Cu<sub>5</sub>FeS<sub>4</sub>, CuFeS<sub>2</sub>, as well as metallic copper and Cu<sub>2</sub>Sb; the possibility of the solidification of the last two components in such systems was noted earlier (Selivanov et al., 2000, 2004). A change in the degree of iron oxidation in the working body does not introduce qualitative changes in the phase composition of the slag but it does affect the interfacial distribution of non-ferrous metals. Copper occurs predominantly in the form of a metal or a sulphide (Fig. 10), and the temperature changes influence their mass ratios. As such, a larger amount of Cu<sub>2</sub>S forms within the temperature range of 700-1100 °C, whereas the production of metallic copper in this temperature range decreases substantially. The reduction of the temperature favours the formation of complex copper sulphides, mainly bornite.

Zinc at high temperatures is represented by the oxide compounds ZnO, ZnFe<sub>2</sub>O<sub>4</sub>, ZnSiO<sub>3</sub> and ZnAl<sub>2</sub>O<sub>4</sub>, the fractions of which decrease as the slag cools down. At low temperatures, the probability of the solidification of zinc sulphide - ZnS - is high.

The samples for investigation have been prepared from a converter slag containing %: 40.7 Fe, 3.0 S, 8.5 Cu, 4.0 Zn, 19.5 SiO<sub>2</sub>, 1.9 CaO, 0.7 MgO, 2.3 Al<sub>2</sub>O<sub>3</sub>, 0.2 Sb, 0.9 Pb, 0.1 As. According to the data of the X-ray diffraction phase analysis, the base phases in the initial converter slag are a fayalite of Fe<sub>2</sub>SiO<sub>4</sub> and a magnetite of Fe<sub>3</sub>O<sub>4</sub>. Copper is mainly detected as bornite and copper sulphide. Zinc is revealed in the form of a sulphide with a sphalerite structure. The melting of the samples followed by rapid cooling decreases the diffraction reflex intensities and preserves the non-equilibrium high-temperature phases. With the cooling of the sample at the rate of 900 °C/s, a significant amount of amorphous phase forms. No reflections of the ZnS phase have been detected at a high cooling rate.

When the initial converter slag sample is subjected to differential thermal analysis during heating in an argon atmosphere (Selivanov et al., 2009a), the following melting-induced endothermic heat effect is observed: it begins at 1079 °C and has a maximum value at 1122 °C (Fig. 11). During its cooling, we established the solidification temperature of the slag melt, which is 1108/1078 °C. According to the mass-spectrometry data, a certain amount of SO<sub>2</sub> precipitates in the heating of the sample (beginning from 300-400 °C), which results

from the interaction of sulphides with the oxides of iron of the highest valence. The slag weight loss upon heating up to 1300 °C is 1.2%.

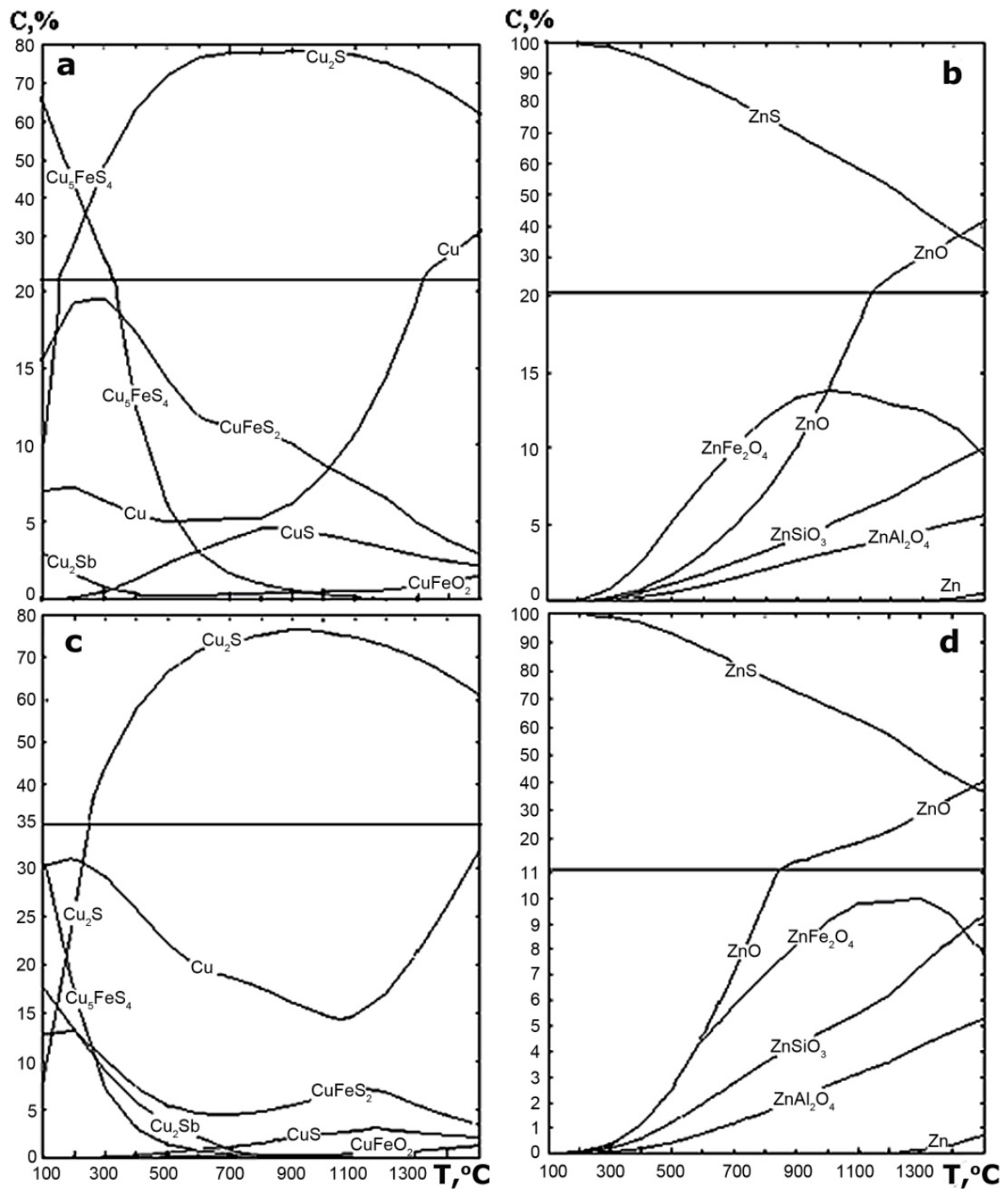


Fig. 10. Distributions (relative %) of copper (a, b) and zinc (c, d) in the components of a condensed phase, depending upon the temperature at the oxidizing degree of iron in the converter slag: 0.4 (a, b) and 0.1 (c, d)

A comparison of the thermograms of the initial slag sample and a sample cooled at a rate of 0.3 °C/s indicates that they are identical. However, a sample cooled at a rate of 900 °C/s is characterized by the appearance of an effect at 533 °C in the DSC curve, which is caused by a second-order phase transformation during devitrification. When this sample is heated further, we detect an exothermic heat effect with an onset/maximum at 608/635 °C. This effect is interpreted as “cold” slag crystallization (ordering its structure). The endothermic effects at 946/963 °C and 1064/1127 °C point to the melting of the sulphide and oxide components of the sample. On the DSC curves of the samples cooled at the rates of 0.3 and 900 °C/s, the solidification effects were equal to 1055/1049 °C and 1085/1072 °C, correspondingly.

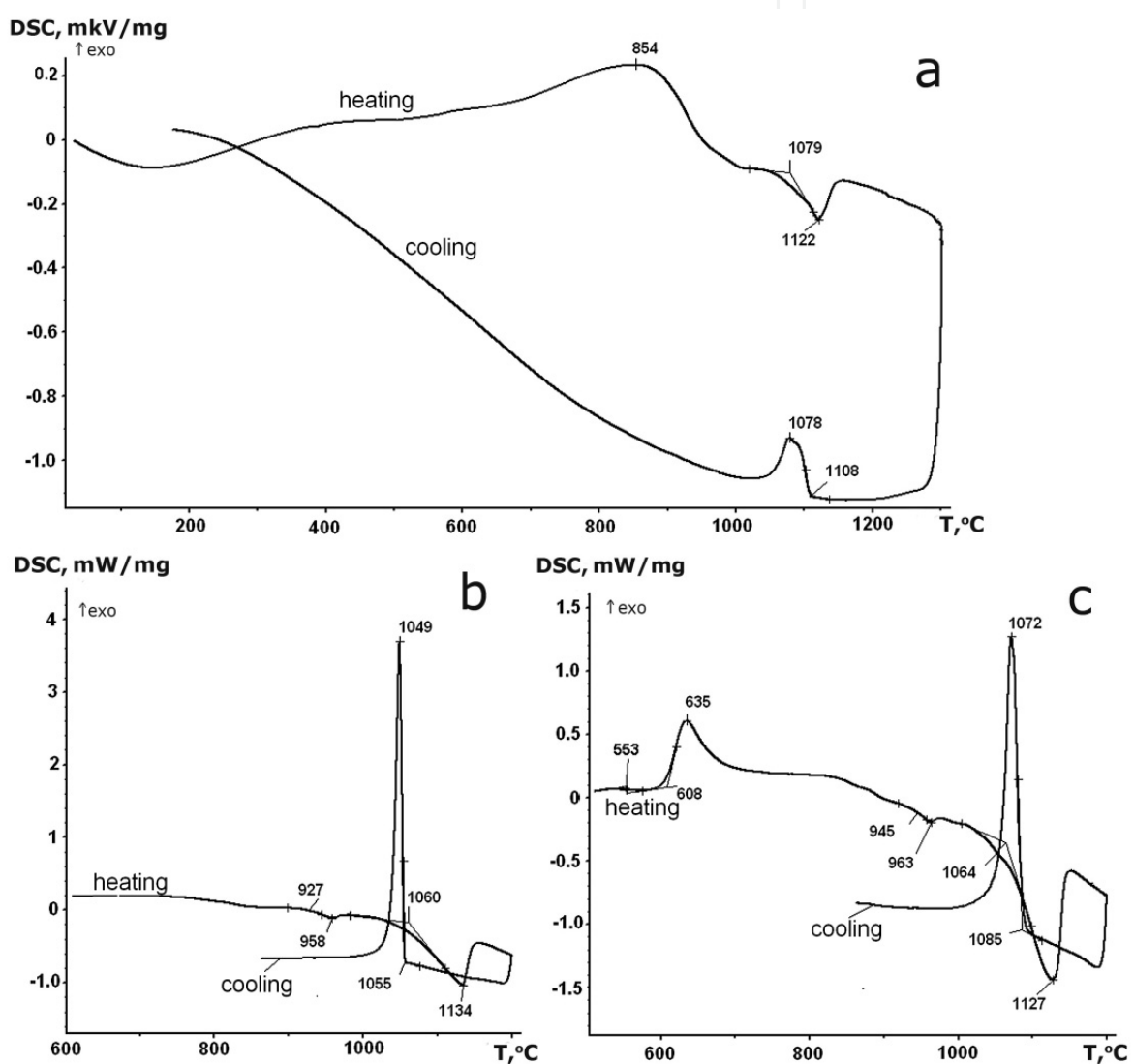


Fig. 11. Sample thermograms of (a) the initial converter slag and the slags that form upon the cooling of the melt at the rates of (b) 0.3 and (c) 900 °C/s

In essence, the temperatures and enthalpies of the thermal effects of the heating of the granulated slags from melts of copper-zinc concentrates and the converting of the matte have similar values (Table 6).

Devitrification			$T_{c.cr.}, ^\circ\text{C}$	$L_{c.cr.}, \text{J/g}$	$L_m, \text{J/g}$		$L_{h.cr.}, \text{J/g}$
$T_{0r}, ^\circ\text{C}$	$T_{gr}, ^\circ\text{C}$	$\Delta c, \text{J/g K}$			1 peak	2 peak	
533	553	0.150	608	66	4	164	157

Table 6. Temperatures and enthalpies of the thermal effects at the heating of the granulated and converter slags

The microstructure of the initial converter slag is represented by iron-silicates and matte particles (Fig. 12). The slag contains a large number of 100  $\mu\text{m}$  magnetite crystals of a regular shape and spherical matte particles smaller than 300  $\mu\text{m}$ . The matte particles have an eutectic structure (copper sulphides, bornite, metallic copper). The silicate constituent of the slag has a small amount of metallic and sulphide copper. These inclusions have sizes equal to 0.1 – 2.0  $\mu\text{m}$  and are concentrated along the boundaries of large iron-silicate aggregates.

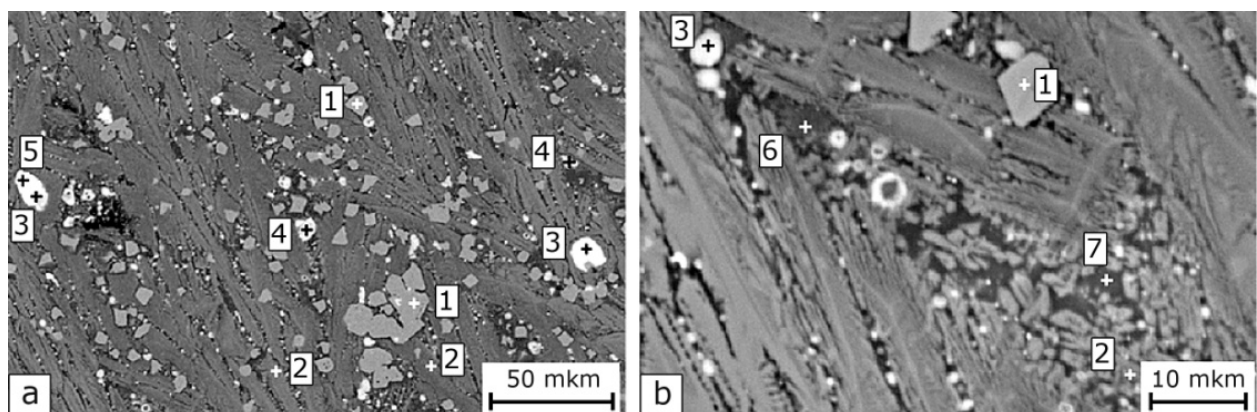


Fig. 12. Microstructure of the sample of industrial converter slag and EPMA points

According to the electron-probe microanalysis of the commercial sample, the iron-silicate phase is heterogeneous in terms of both major (iron, silicon) and dissolved impurities (Table 7). The calculated composition of the iron-silicates ranges from  $\text{Fe}_{0.94}\text{SiO}_{2.94}$  to  $\text{Fe}_{1.59}\text{SiO}_{3.59}$ . The iron-silicates contain 0.5–2.0  $\text{Al}_2\text{O}_3$ , 0.5–1.0  $\text{MgO}$ , 0.2–0.5  $\text{K}_2\text{O}$ , 0.2–1.1  $\text{CaO}$ , 5.3–6.6  $\text{Zn}$ , and 0.1–0.6%  $\text{S}$ . Moreover, we detected a silicate phase that corresponds to the  $\text{SiO}_2\text{-FeO-CaO-Al}_2\text{O}_3\text{-Zn(Pb)O}$  system and has a low iron content with a high calcium content. The magnetite crystals (61.4–63.3%  $\text{Fe}$ ) located in the plane of the section contain the following impurity elements: 1.2–1.3  $\text{Al}$ , 0.4–1.2  $\text{Si}$ , 0.3–0.2  $\text{Ti}$ , 0.1–2.5  $\text{Cr}$  and 2.7–3.2%  $\text{Zn}$ . The sulphide phases in the slag are represented by bornite- and sphalerite-based solid solutions. The copper content in the bornite solid solution is lower than the stoichiometric copper content. The  $\text{ZnS}$ -based phase (sphalerite) contains 37.9–53.3  $\text{Zn}$ , 0.9–7.3  $\text{Cu}$ , 11.5–21.6%  $\text{Fe}$ , and a near-stoichiometric sulphur content. The regions of the  $\text{PbS-Cu}_2\text{S-FeS}$  solid solution are located along the periphery of the sulphide phases.

The base of the slag sample cooled at the rate of 0.3  $^\circ\text{C/s}$  also consists of iron-silicate phases, magnetite and sulphides (Fig. 13). The re-melting and slow cooling of the slag result in a significant coarsening of the formed crystals. The area of its polished section is a mainly occupied silicate phase with a composition close to  $\text{Fe}_{1.59}\text{SiO}_{3.59}$ ; between them there are small  $\text{Fe}_{1.12}\text{SiO}_{3.12}$  dendrites and calcium- and silicon-rich phases (Table 8). Apart from iron, the magnetite also contains zinc, titanium, silicon and aluminium impurities as in the initial converter slag.

№ point	Content, mas. %													Phases
	Mg	Al	Si	S	K	Ca	Ti	Cr	Fe	Cu	Zn	Pb	O	
1	-	1.2-1.3	0.4-1.2	-	-	0.1	0.2-0.3	0.1-2.5	61.4-63.3	-	2.7-3.3	-	30.4-30.8	Fe <sub>3</sub> O <sub>4</sub>
2	0.3-0.6	0.3-1.0	13.8-17.0	0.1-0.6	0.1-0.3	0.1-0.8	-	-	38.1-43.9	-	4.3-5.3	-	36.5-38.3	Iron-silicate
3	-	-	0.3	26.2-27.6	-	0.1	-	-	17.0-20.8	50.1-55.1	0.3-0.4	1.0-1.2	-	Cu <sub>5</sub> FeS <sub>4</sub> solid solution
4	-	до 0.5	0.4-3.4	30.0-32.7	0.1	0,2	-	-	11.5-21.6	0.9-7.3	37.9-53.3	-	-	(Zn,Fe,Cu)S
5	-	-	0.2	16.6	-	-	-	-	9.4	23.4	0.6	49.8	-	(Pb,Cu,Fe)S
6	-	3.0	17.7	0.4	0.7	0.9	0.4	-	33.2		3.5	0.6	39.4	Fe <sub>0,94</sub> SiO <sub>3,47</sub>
7	0.3	4.6	21.9	1.6	0.2	6.3	0.4	-	14.6	0.5	4.4	3.1	42.1	Iron-silicate

Table 7. EPMA data on the phase composition of the initial converter slag (according to Fig.12)

The coarse sulphide particles of a size of 15–30 µm consist of bornite - the composition of which varies from Cu<sub>7,2</sub>FeS<sub>6,4</sub> to Cu<sub>3,2</sub>FeS<sub>3,3</sub> - and a PbS–Cu<sub>2</sub>S–FeS alloy (Fig. 13). The bornite is located in the centres of the particles, while the lead-containing sulphide alloy with a lower melting point forms on the fringes on its surface.

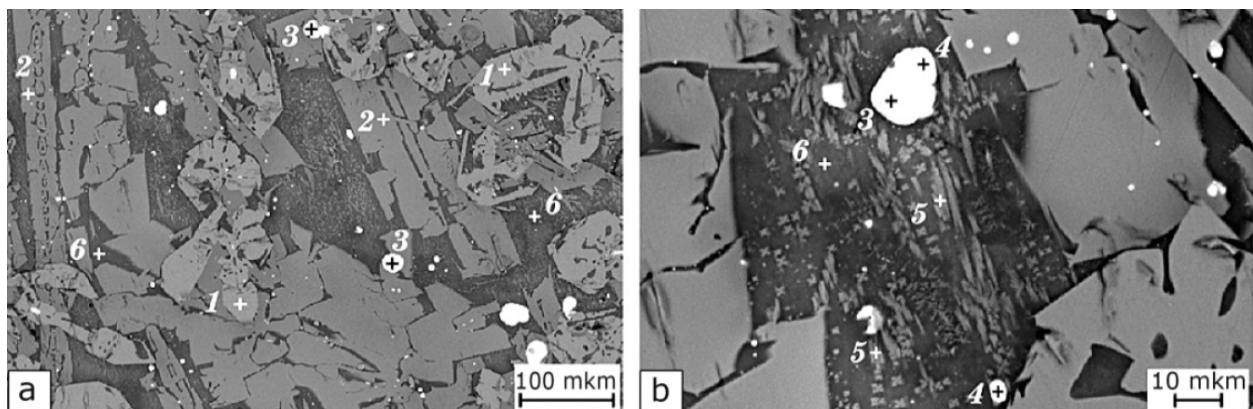


Fig. 13. The sample microstructure of the converter slag cooled at a rate of 0.3 °C/s and EPMA points

The structure of the slag sample cooled at a rate of 900 °C/s is represented by glass, magnetite, iron-silicate phase crystals and sulphide inclusions of a spherical form up to 10 µm (Fig. 14). According to the EPMA data (Table 9), the glass has about 36% SiO<sub>2</sub> and 51% FeO<sub>1+x</sub>. Acicular crystals 5–15 µm long and about 1 µm thick are clearly visible against the background of the glass; their composition is close to that of iron-silicate of Fe<sub>3,4</sub>SiO<sub>4,4</sub>. Magnetite (60.4–61.6% Fe) is present in the form of dendrites. The sulphide phase (its coarsest particle is 6.4 µm in size) is inhomogeneous and its central portion corresponds to the formula of Cu<sub>5,4</sub>FeS<sub>3,4</sub>. The distribution of nonferrous metals in the sulphide particle is also non-uniform: the centre contains 6.2% Zn, 1.6% Pb, and 1.4% As, and the periphery contains 1.3% Zn, 2.0% Pb and 4.7% As.

№ point	Content, mas. %									Phases
	Al	Si	S	Ca	Fe	Cu	Zn	Pb	O	
1	2.4-2.5	0.4	-	0.1	63.3	-	2.4-2.5	-	30.8	Fe <sub>3</sub> O <sub>4</sub>
2	-	15.0	-	0.3	42.1-42.9	-	3.4	-	37.2-37.3	Iron-silicate
3	-	0.2-0.5	21.5-28.5	0.1	8.2-14.9	55.4-69.2	0.3	0.5-0.6	-	Cu <sub>5</sub> FeS <sub>4</sub> solid solution
4	-	0.3-0.8	18.8-18.9	0.1-0.2	9.3-13.1	23.4-25.3	0.5-0.8	40.6-47.8	-	(Pb,Cu,Fe)S
5	2.4-2.7	16.4-16.9	0.4	1.9-2.1	32.0-33.4	< 0.2	5.3-5.5	0.9-1.0	38.1-38.5	Iron-silicate
6	5.8-7.2	19.9-22.5	0.6-1.1	5.7-6.9	13.0-15.3	-	3.9-6.2	2.3-2.7	40.7-42.5	Iron-silicate

Table 8. EPMA data on the phase composition of the converter slag cooled at a rate of 0.3 °C/s

This data indicates that an increase in the cooling rate leads to vitrification. However, even at a cooling rate of 900 °C/s an iron-silicate phase and magnetite solidify and sulphides precipitate. The compositions of the iron-silicate crystalline phases vary over wide limits: as the cooling rate increases, high-iron modifications form and the fraction of magnetite

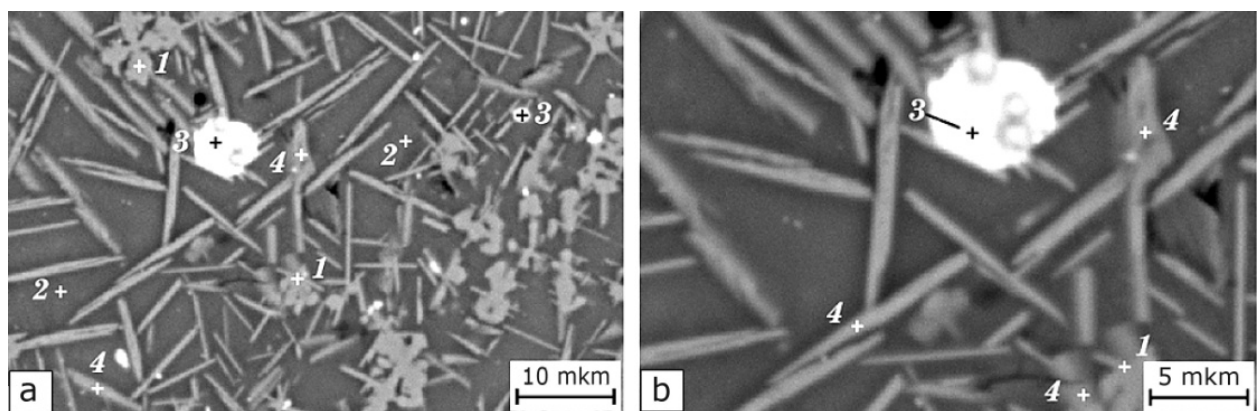


Fig. 14. Microstructure of the converter slag cooled at a rate of 900 °C/s and EPMA points

№ point	Content, mas. %										Phases
	Al	Si	S	Ti	Fe	Cu	Zn	Pb	O	As	
1	2.7-3.1	1.4	-	0.2	60.4-61.1	-	2.4-2.5	0.1	31.4-31.5	-	Fe <sub>3</sub> O <sub>4</sub>
2	2.3-2.6	15.5-17.3	0.8-0.9	0.1	34.2-41.0	0.2	4.7-5.4	0.9	28.0-38.1	0.3	Glass
3	-	0.3-0.9	17.2-20.3	-	9.8-10.8	62.6-64.8	0.4-6.2	0.9-2.0	-	0.6-4.7	Cu <sub>5</sub> FeS <sub>4</sub>
4	1.5-1.9	7.4-7.8	0.2-0.3	0.1	51.1-51.3	0.2-0.03	3.2-3.4	0.2-0.3	34.0-34.1	<0.1	Iron-silicate

Table 9. EPMA data on the phase composition of the converter slag cooled at rate of 900 °C/s (according to Fig. 14)

crystals decreases. A decrease in the cooling rate of the slag is accompanied by magnetite formation (endothermic effect) and the precipitation of iron-silicate crystals with a lower (compared to glass) iron content.

According to the EPMA data, none of the samples contains a phase close to stoichiometric fayalite ( $\text{Fe}_2\text{SiO}_4$ ). The whole set of the iron-silicate phases that form during the slow cooling of the converter slag corresponds to an Fe/Si atomic ratio of 0.9–1.6. The cooling of the slag at the high (900 °C/s) rate is a result of the increase in this ratio to 3.4. A decrease in the cooling rate of the molten slag favours an increase in the fraction and sizes of magnetite crystals and sulphide particles. The distribution of non-ferrous metals between phases changes according to the fraction of the sulphides.

Copper is concentrated in the bornite-based solid solution, which forms in all the samples. The bornite content increases as the cooling rate decreases, which can be explained by the specific features of the solidification and separation of oxide–sulphide systems that are related to changes in the sulphides' solubilities. The results obtained agree with the TDS data with regard to the predominant formation of copper sulphides during the cooling of the slag. We failed to detect metallic copper in real slags, irrespective of the cooling rate (see Fig. 10). During slag solidification, zinc is distributed between oxide and sulphide phases. An individual (Zn,Fe)S phase containing 38–53% zinc was revealed only at the low cooling rate. Lead in the slag is present in both oxide and sulphide forms. Its content in the iron-silicate phase correlates (increases) with the silicon dioxide content. Lead forms the regions of a sulphide phase (40–48% Pb) of 1–2  $\mu\text{m}$  in size at the low cooling rate. The formation of the oxide compounds of zinc and lead supports the absence of an equilibrium state in all of the investigated slag samples. Sulphide phases have a high arsenic content. The arsenic content in a bornite-based solid solution reaches 4.7% in a slag sample cooled at a rate of 900 °C/s and the arsenic content in iron-silicates is 0.1%.

Thus, when changing the cooling rate of the slag, we can affect the forms of copper, zinc, arsenic and lead in it in order to prepare the slag for the additional recovery of precious metals (Selivanov, 2009a). Moreover, the slag cooling conditions affect the composition of the iron-silicate forming phases, and its properties control the energy consumed for grinding as well as the possibility of using magnetic separation methods for the precipitation of iron oxides, and so on. The converter slag contains both mechanically-introduced coarse matte particles and fine sulphides, which precipitate during the solidification of an oxide–sulphide melt. The cooling rate of the molten slag controls both the phase composition and the particle size of the oxide and sulphide forming phases. The oxide component transforms into a glassy state at a high (900 °C/s) cooling rate of the slag. The devitrification and cold crystallization of the glass falls within the temperature range of 533 – 635 °C.

The copper in the slag is mainly represented by the bornite-based solid solution, the content of which increases as the cooling rate decreases. Zinc and lead are distributed between the oxide and sulphide components. The individual sulphides of these metals are only revealed with the low cooling rates of the slag.

## **5. Forms of metals finding in the slag of combined melting – The converting of copper concentrates**

The autogenous processes of the converting of copper-containing raw materials, including the application of both «Noranda» and combined melting–converting (CMC) units have

been widely used in non-ferrous metallurgy. However, the copper content in the slags which are formed during the smelting of concentrates in these units is rather large. In order to decrease the loss of metals and to choose the methods of the processing of slags, it is of the prime importance to reveal the forms of the existence of the precious components in them. The molten slags are - in their compositions - close to the  $\text{FeO}_x\text{-SiO}_2$  system and, at the temperatures corresponding to pyrometallurgical processes, agree with homogeneous melts (Vanyukov & Zaitsev, 1969, 1973). During slag cooling, a number of micro-processes connected with compound crystallization, liquation phenomena and the change of the detection of forms of non-ferrous metals occurs (Kukoev et al., 1979). The last of these, in turn, determine the choice of methods for the re-extraction of precious components from the slag.

As a starting sample - the slag of a pilot unit of CMC cooled at a rate of about  $0.5\text{ }^\circ\text{C}/\text{min}$  (Selivanov et al., 2004). According to the data of the chemical analysis, the slag contained, %: 1.2 Cu, 55.9  $\text{Fe}_{\text{total}}$ , 4.9  $\text{Fe}^{3+}$ , 53.3  $\text{Fe}^{2+}$ , 0.4  $\text{Fe}_{\text{met}}$ , 3.1 S, 16.0  $\text{SiO}_2$ , 3.6 Zn, 0.1 Pb, 0.1 As, 0.1 Sb, 0.5 CaO and 0.5  $\text{Al}_2\text{O}_3$ . The studied slag sample in its chemical composition is close to the slag of copper matte converting. The relatively high sulphur content in the slag allows it to be referred to the oxide-sulphide melts class, the crystallization of which must be accompanied by a number of complex interactions changing the form of the metals' detection (Kukoev et al., 1979; Selivanov et al., 2000).

The thermodynamic modelling of the processes (Moiseev & Vyatkin, 1999; Selivanov et al., 2004) occurring during slag cooling was carried out for the working body and is in substantial agreement with the slag composition taken for the investigation. The thermodynamic functions of elements and compounds in the condensed ( $\text{Cu}$ ,  $\text{Cu}_2\text{O}$ ,  $\text{CuO}$ ,  $\text{CuFe}_2\text{O}_4$ ,  $\text{Cu}_2\text{Fe}_2\text{O}_4$ ,  $\text{Cu}_2\text{S}$ ,  $\text{CuFeS}_2$ ,  $\text{Cu}_5\text{FeS}_4$ ,  $\text{Cu}_3\text{As}$ ,  $\text{Cu}_2\text{Sb}$ , Zn, ZnO, ZnS,  $\text{ZnSiO}_3$ ,  $\text{Zn}_2\text{SiO}_4$ ,  $\text{ZnAl}_2\text{O}_4$ ,  $\text{ZnFe}_2\text{O}_4$ ,  $\text{Fe}_{\text{met}}$ , FeO,  $\text{Fe}_3\text{O}_4$ ,  $\text{Fe}_2\text{O}_3$ , FeS,  $\text{FeS}_2$ ,  $\text{FeSiO}_3$ ,  $\text{Fe}_2\text{SiO}_4$ ,  $\text{FeAl}_2\text{O}_4$ ,  $\text{Fe}_2\text{ZnO}_4$ , Pb, PbO,  $\text{Pb}_2\text{O}_3$ , PbS,  $\text{PbSiO}_3$ , As,  $\text{As}_2\text{O}_3$ ,  $\text{As}_2\text{O}_5$ ,  $\text{As}_2\text{S}$ ,  $\text{As}_2\text{S}_3$ , Sb,  $\text{Sb}_2\text{O}_3$ ,  $\text{Sb}_2\text{O}_5$ ,  $\text{Sb}_2\text{S}$ ,  $\text{Al}_2\text{O}_3$ ,  $\text{Al}_2\text{SiO}_5$ ) and gaseous ( $\text{S}_2$ ,  $\text{SO}_2$ ,  $\text{SO}_3$ , Zn, ZnO,  $\text{N}_2$ ,  $\text{O}_2$ , Pb, PbS,  $\text{As}_2\text{O}_3$ ,  $\text{As}_2\text{O}_5$ ,  $\text{Sb}_2\text{O}_5$ ,  $\text{Sb}_2\text{O}_3$ , etc.) states have been used for the calculations. The modelling was carried out during the changing of the temperature from 1520 to  $25\text{ }^\circ\text{C}$  with steps of 50 degrees.

According to the TDS data, slag cooling leads to the changing of the parts of phases and the forms of the metals which exist (Fig. 15). Accordingly, the working body temperature decrease increases the crystallization probability of  $\text{FeSiO}_3$  and  $\text{Fe}_2\text{SiO}_4$  iron-silicate compounds and favours magnetite formation, which can be explained by the disproportionate amount of iron oxide (II) and by the interactions between non-ferrous metals oxides and iron oxide:



For the non-ferrous metals in the slag, one would expect the changing of their forms of existence at the expense of reactions between sulphides and oxides (Belyaev et al., 2001; Spira & Themelis, 1969). If, at a high temperature, the copper in the slag is preferably in the form of sulphide, then cooling can lead to its transition into its metallic state:



The working body (slag) cooling favours a  $\text{ZnO} \rightarrow \text{ZnS}$  transformation according to the reaction:



This means that copper, antimony and arsenic are the most electropositive metals for the problem at hand and one should also expect the formation of Cu-Sb-As alloys as well as copper.

Iron-silicates and oxides, as well as bornite, were found in the slag by way of X-ray diffraction analysis (Fig. 16) and they were identified on the basis of the data from (PC-PDF, 2003) for  $\text{Fe}_2\text{SiO}_4$ ,  $\text{FeO}$ ,  $\text{Cu}_5\text{FeS}_4$  and  $\text{Fe}_7\text{SiO}_{10}$ . Some discrepancies in the X-ray reflexes between their meanings for pure compounds is suggestive of the formation of solid solutions which distort the minerals' lattice.

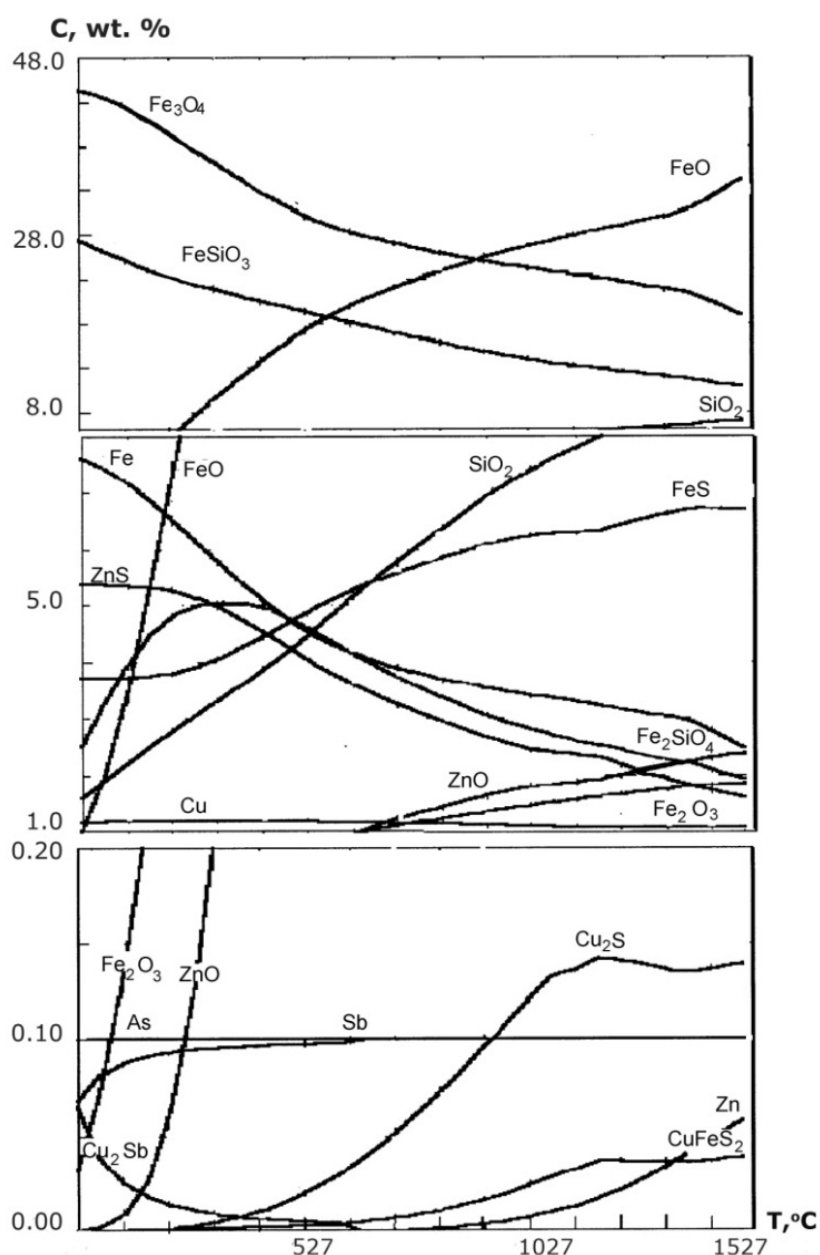


Fig. 15. Changing of the forms of metals present in the CMC slag according to the TDM data

The main structural components of a slag are fayalite and an iron-silicate phase with a high FeO content (Fig. 17). Fayalite, which is close to  $\text{Fe}_n\text{SiO}_{2+n}$  in composition, is presented by a solid solution of iron, zinc and calcium silicates. The iron-silicate phase (83% FeO) conforms to the  $n\text{FeO} \cdot m\text{SiO}_2$  formula. The micro-hardness of fayalite varies within the limits of 5300 to 8400 MPa but that of the micro-hardness of the iron-silicate phase within the limits of 4100 to 6100 MPa. Apart from the main phases in the slag, we have revealed iron oxides with a micro-hardness of 5100 to 8400 MPa, which exceeds the values characteristic of pure wustite ( $\sim 4300$  MPa), iron sulphides which deposit in the form of FeS troilite (2440-2800 MPa) and FeS-FeO eutectic (3400 to 4900 MPa) of different dispersivity, zinc ferriferous sulphides (christophite) and, in lesser amounts, bornite and a solid solution on its base.

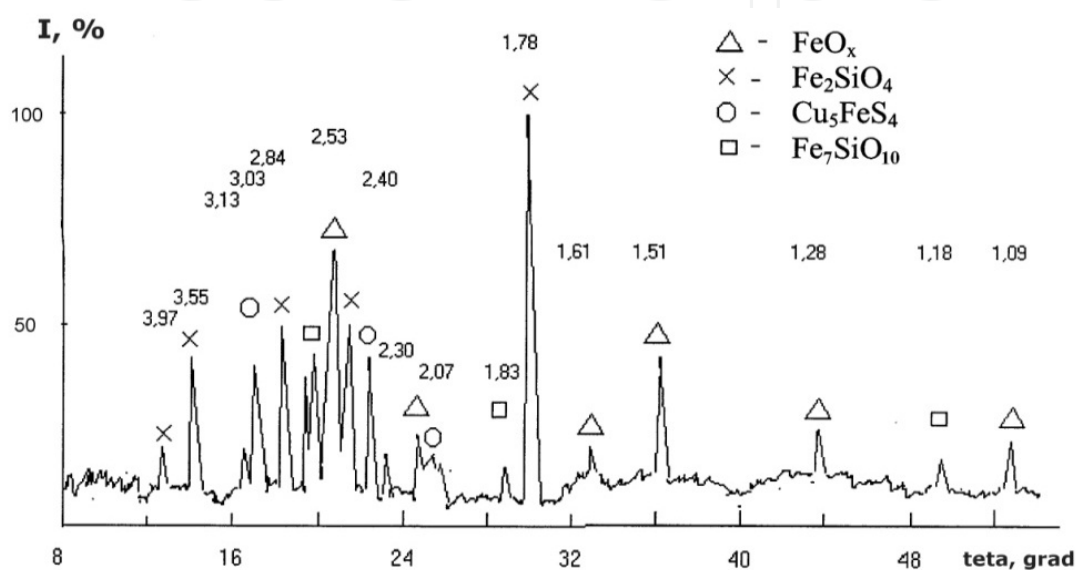


Fig. 16. X-ray diffractogram of the CMC slag

The crystallization of slag containing 16% silica, according to the diagram of the FeO-SiO<sub>2</sub> condition, proceeds from a temperature of 1250 °C and is accompanied by the rejection of iron-silicate phase crystals and excess wustite (Selivanov et al., 2004). X-ray spectral microanalyses of the slag (Fig. 18) enable us to establish the composition of the phase components (Table 10). As follows from the data obtained, the oxide and iron-silicate phases do not contain copper. A small quantity of non-ferrous metals (Zn, As - 0.2%) was dissolved in the FeO<sub>x</sub> phase. Unlike FeO<sub>x</sub>, the silicate phases (the first - with 13.4% and the second - with 5% of Si) have a zinc content of up to 3 - 4%. The silicate phases conform to compositions of Fe<sub>2</sub>SiO<sub>4</sub> (fayalite) and Fe<sub>7</sub>SiO<sub>10</sub> (a solid solution with a high content of FeO).

Non-ferrous metals are preferably concentrated in metallic (a size up to 40 μm) and sulphide (up to 100 μm) inclusions. The metallic phase is represented by a Cu-Sb alloy with Sn (3-5%), As (5 - 10%) and Ni (1 - 7%) dissolved in it. The sulphide phases are formed with the participation of Cu, Zn and small quantities of Pb (0.2-0.8%) and As (0.2%). A conglomerate of sulphides and wustite occurs between the crystals of fayalite, and this conglomerate is revealed in the part of the section which is sized 200 μm (Fig. 18). There is a Cu-Sb particle in the centre of the conglomerate. The composition of this particle changes from the surface to the centre. The surface of the particle contains 50% copper and about 30% of Sb, whereas the internal part is more than 50% of the antimony. The heterogeneity of the particle is seen in the micro-structure obtained by the absorbed electrons during X-ray spectral

microanalysis. The coefficients of distribution during liquation ( $K_l$  – the proportion of elements contents in copper  $[C]_{Cu}$  and antimony  $[C]_{Sb}$  parts) have the following meanings:

Element	Cu	Fe	Sb	Zn	Pb	Sn	Ni	As
$K_l = [C]_{Cu} / [C]_{Sb}$	10	0.2	0.5	0.5-1.0	0.5	1.2-2.5	0.2-0.4	0.3-0.5

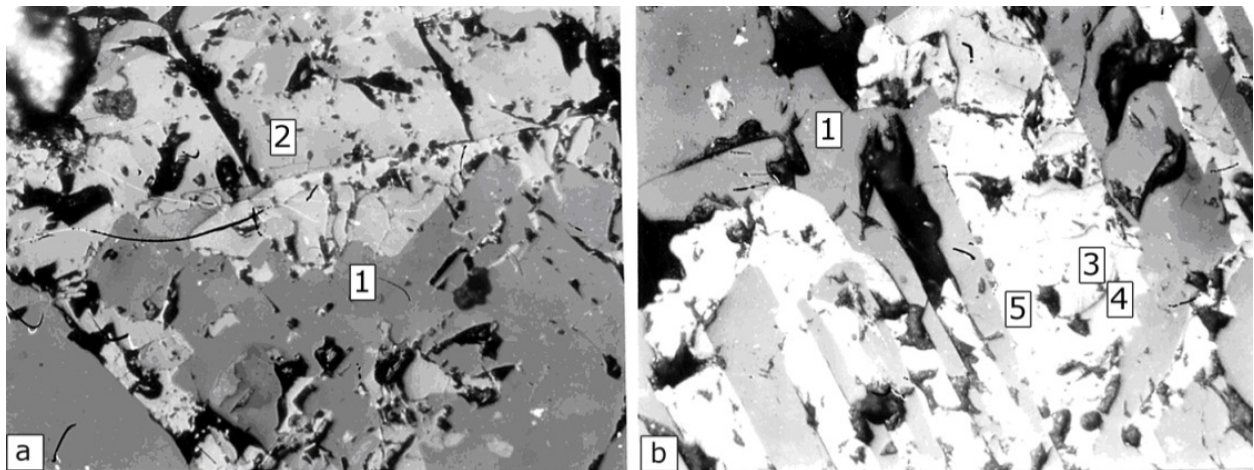


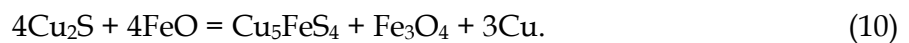
Fig. 17. Microstructure of the CMC slag : a) – x100; б) – x 200: 1 – fayalite, 2 – iron-silicate phase, 3 – wustite, 4 – christophite, 5 – eutectic of FeS-FeO

Scanning the area revealed that the sulphide-metallic part in the section space (Fig. 18) consists of a conglomerate of copper, zinc and iron sulphides as well as an intermetallic phase, closely conforming to the  $Cu_6Sb$  composition. The metallic phases stand out in close proximity or else together with wustite and sulphides. The phases are basically solid solutions and contain a significant proportion of impurities. Solid solutions of iron and zinc sulphides are enriched with copper (0.3-3.1%) in contrast with oxide-silicate phases.

As is known, zinc, iron sulphides and FeO are isolated during cooling from FeO-ZnS melts, having unlimited solubility in the liquid state (Kopilov et al., 2002; Toguzov et al., 1982). Apart from this, the double FeO-ZnS eutectic and below at a temperature 920 °C, a threefold FeO-FeS-ZnS eutectic crystallizes from the high-sulphurous residual melt. The last eutectic has the theoretical composition, %: 61.0 FeS, 36.0 FeO, 2.5 ZnS. During slow cooling, the formation of both the threefold and the double eutectic FeS-FeO and FeO-ZnS is possible. In the investigated sample, the FeO-ZnS eutectic is represented by christophite and wustite, which were evolved in turn, and the FeS-FeO eutectic by the primary troilite and wustite of a different dispersion (Fig. 17). Close contact with christophite and wustite in the field of the section confirms the progress of the reaction (9).

Complete (solidus) sulphide crystallization initiates at a temperature below 850 °C, with the formation of another threefold eutectic (30%  $Cu_2S$ , 45% FeS and 25% FeO) consisting of FeO, FeS and a solid solution of bornite. In cooling, the solid solution of bornite dissociates - partially or fully - forming a lattice structure of a chalcopyrite decomposition in bornite. The conglomerate illustrated in Fig. 18 is demonstrated by a bornite solid solution, a ferrous sulphide of zinc and copper, troilite, wustite and christophite, which provides evidence of both threefold eutectics. The phase components of the threefold eutectics are more dispersed than those of the double ones.

From the phase diagram of FeO-Cu<sub>2</sub>S it follows that copper sulphide is soluble in those oxide melts containing FeO, but if the temperature is below 1100 °C then the interaction of the components with the formation of a solid solution of bornite, metallic copper and iron oxide occurs, which is due to the course of the reaction:



In Fig. 18 Sulphide and metallic phases are represented by metallic copper as Cu<sub>6</sub>Sb, with two kinds of sulphides containing iron, bornite and wustite as well.

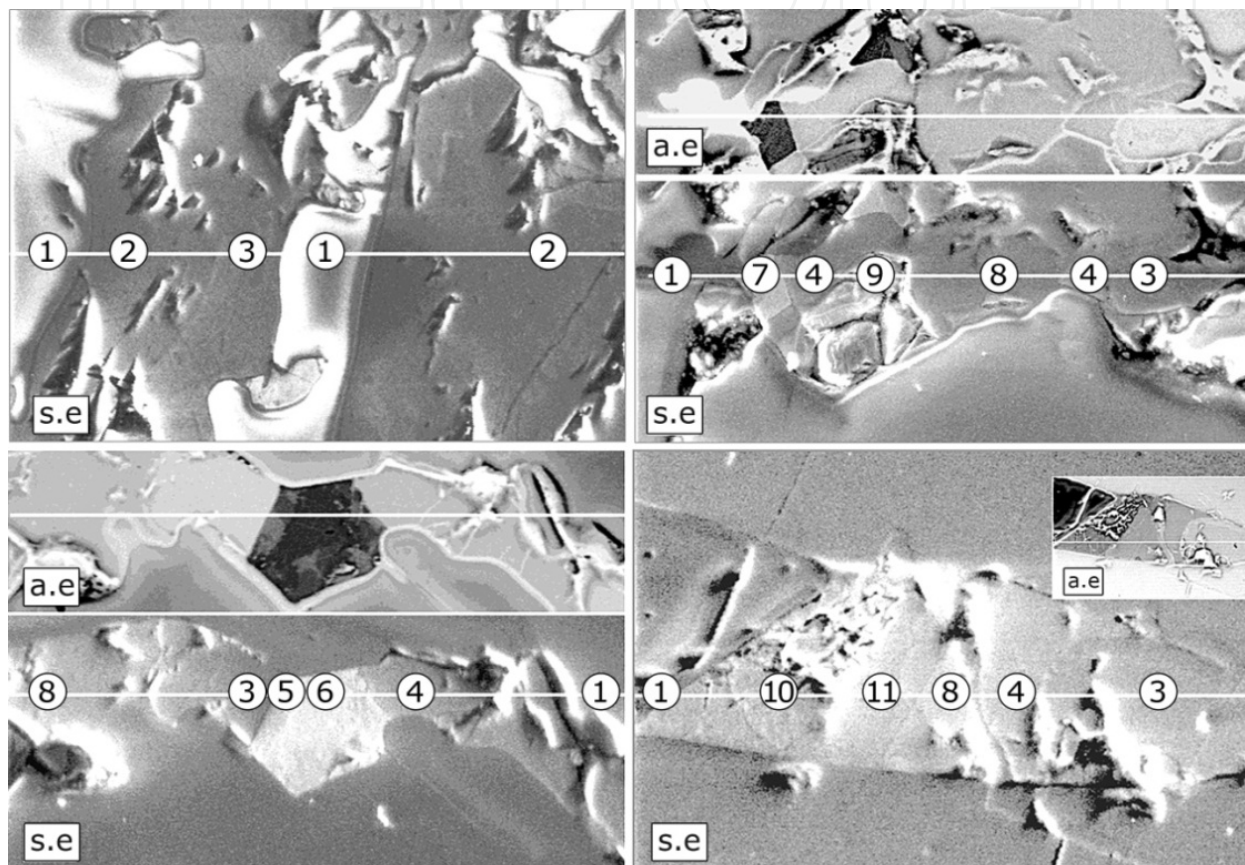


Fig. 18. Structure of the CMC slag in the absorbed (a.e.) and secondary (s.e.) electrons in the sections of 200 μm: 1 - Fe<sub>2</sub>SiO<sub>4</sub>; 2 - Fe<sub>7</sub>SiO<sub>10</sub>; 3 - FeO<sub>x</sub>; 4 - FeS; 5 - Cu-Sb alloy (the particle surface), 6 - Sb-Cu alloy (the particle centre), 7 - Cu<sub>6</sub>Sb; 8 - (Fe, Zn)S; 9 - Cu<sub>5</sub>FeS<sub>4</sub>, 10 - a solid solution on the base of the bornite, 11 - a solid solution of copper and zinc sulphides

Proceeding from the composition (according to the EPMA data) of clearly marked crystals, the phases containing copper correspond to Cu<sub>4.4</sub>FeS<sub>3</sub>, 2 and Cu<sub>5</sub>FeS<sub>4</sub>, the phases containing zinc to Zn<sub>0.4</sub>Fe<sub>0.6</sub>S and the iron sulphide phase to FeS. The coefficient of the elements' distribution between the sulphide phases has the following meanings (K<sub>b/t</sub> and K<sub>c/t</sub> - the coefficients of the distribution are determined as the ratio of the metals' content in the bornite/troilite and christophite/troilite phases):

Element	Cu	Zn	Pb	Ni	As
K <sub>b/t</sub>	104 - 149	2.5 - 5.0	1.8	2 - 5	1 - 2
K <sub>c/t</sub>	1 - 3	1.5 - 2.5	0.6 - 0.9	1 - 3	1 - 3

Thus, the slag melts of the integrated melting-converting of copper concentrates refer to oxide-sulphide systems' crystallization, which is accompanied by a phase transformation characteristic of both oxide and sulphide systems. Besides this, the phase changes fraught with the interaction of oxides and sulphides proceed in oxisulphide systems, resulting in the extraction of metals and oxide-sulphide eutectics.

The oxide component of slowly cooled slag is represented by the solid solutions of iron oxides and iron-silicates. The number of non-ferrous metals dissolved in them (apart from zinc) is less than a tenth part of one percent. The cooling and crystallization of slag leads to the concentrating of non-ferrous metals in metallic and sulphide phases. The metallic phase is represented by Cu-Sb alloy with Fe, Ni, Sn, As and other elements dissolved in it. The metallic phase serves as the collector of non-ferrous metals and contains up to 50% antimony. In separating the metal from the solid slag by the methods concentration (flotation, gravitation, etc.) one should take into account the formation of copper alloys but not copper, as has been assumed before.

№ point	Content, mas, %											Phases
	Fe	Cu	Ni	Zn	S	Sb	Pb	Sn	Si	As	Ca	
1	50.9	0	0	3.5	0	0	0	0	13.4	0	0.9	Fe <sub>2</sub> SiO <sub>4</sub>
2	64.7	0	0	3.3	0	0	0	0	5.0	0	0.1	Fe <sub>7</sub> SiO <sub>10</sub>
3	76.4	0	0	0.2	0	0	0.1	0	0.2	0.1	0.1	FeO <sub>x</sub>
4	62.5	0.4	0	0.1	36.4	0	0.3	0	0.1	0	0	FeS
5	3.7	50.9	0.9	0.2	0.2	29.2	0.1	5.5	0.1	5.7	0.1	Cu-Sb (surface)
6	21.7	4.8	7.2	0.4	0.1	50.2	0.3	2.7	0.1	10.7	0.1	Sb-Cu (centre)
7	0.9	60.5	3.3	0.4	0.1	23.8	0.1	6.7	0.3	3.0	0.1	Cu <sub>6</sub> Sb
8	37.3	0.3	0.1	27.2	34.2	0	0.3	0	0	0	0	(Zn,Fe)S
9	12.6	62.6	0.1	0.3	23.3	0.1	0.6	0	0	0.2	0.1	Cu <sub>5</sub> FeS <sub>4</sub>
10	21.5	56.4	0.1	0.4	20.8	0	0.8	0	0.1	0.1	0.1	Cu <sub>5</sub> FeS <sub>4</sub> solid solution
11	27.8	11.0	0.1	27.4	31.2	0	0.3	0	0	0.1	0.1	Solid solution of copper and zinc sulphides

Table 10. The composition of phases identified in the CMC slag (Fig. 18)

The sulphide phases are represented mainly by solid solutions containing copper, iron, zinc and small amounts of lead and arsenic as well. The main phases are bornite, christophite, troilite and the products of the eutectics' decomposition. The size of the metallic and sulphide phases in the slag amounts to 10 - 100 µm, which will allow their breakdown to be carried out by way of grinding with the standard equipment.

## 6. Peculiarities of the crystallization of high-magnesian iron-silicate slags

The processing of oxide nickel ores with the smelting technique for mattes is connected with the formation of a great amount of high-magnesian silicate slags. The investigations presented here are devoted to the study of forms for finding metals and structures of granulated slags of nickel production which are in substantial agreement with the SiO<sub>2</sub>-

FeO<sub>x</sub>-MgO-CaO system, with the phase transformations' peculiarities occurring during their heating as well as during their crystallization during the course of annealing.

The commercial slag sample of the shaft smelting of oxide nickel ores from "Ufaleynickel" JSC (Russia, Ural), obtained by way of the granulation of an oxide melt in the water pond and containing, %: 13.0 MgO, 42.1 SiO<sub>2</sub>, 20.8 Fe, 7.2 CaO, 5.8 Al<sub>2</sub>O<sub>3</sub>, 0.2 Ni, 0.3 S, was taken for investigation (Sergeeva et al., 2011). The sample slag annealing was carried out in a furnace by heating it up to 1000 °C and upon the subsequent maintenance of this temperature for 60 minutes.

The results of the X-ray-phase analysis showed that the initial granulated sample of slag almost completely consisted of glass (Fig. 19). There are no reflexes conforming to crystal phases in the diffractogram. Responses conforming to Ca(Mg,Fe)Si<sub>2</sub>O<sub>6</sub> diopside and (Fe,Mg)<sub>2</sub>SiO<sub>4</sub> fayalite, with the structure of olivine, were revealed in the slag diffractogram after the annealing.

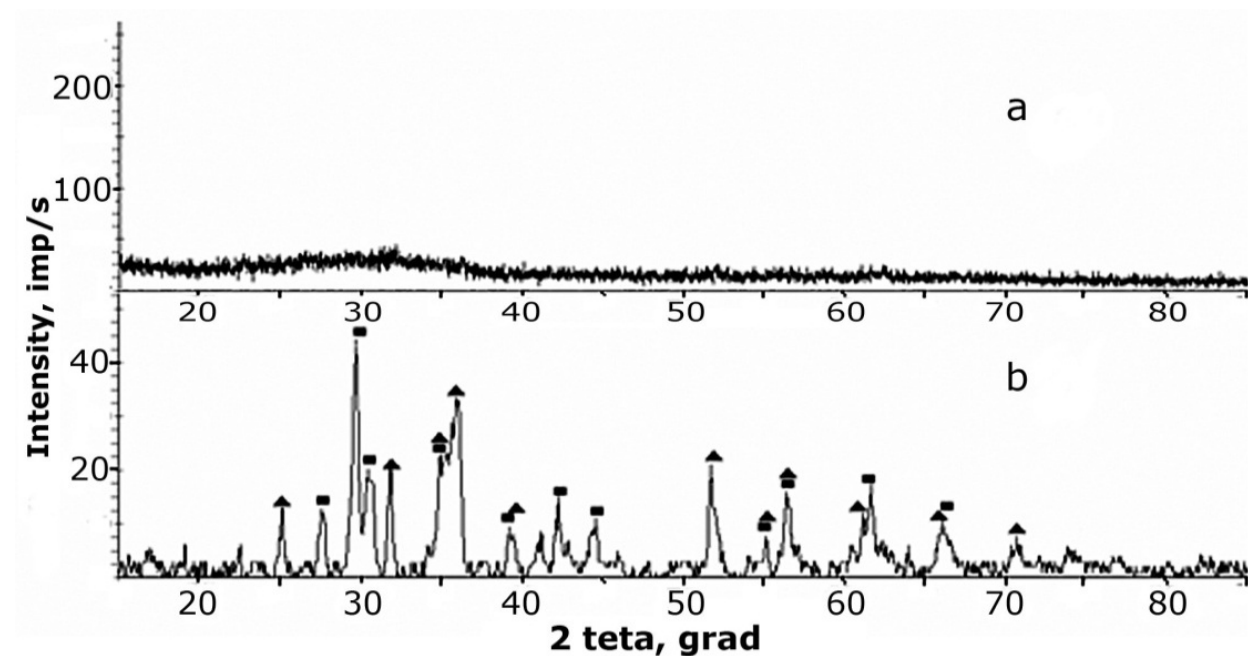


Fig. 19. Slag diffractograms: a - initial, granulated; b - after annealing: ■ - Ca(Mg,Fe)Si<sub>2</sub>O<sub>6</sub>; ▲ - (Fe,Mg)<sub>2</sub>SiO<sub>4</sub>

During the heating (20 °C/min) of the granulated slag in the argon flow on the curve of the heat flow, we revealed the effect at 646 °C due to the phase transition of the second sort's conformity to the process of devitrification (Fig. 20). The heat capacity change of devitrification was equal to 0.513 J/(g·K). A complex exothermic effect beginning at 744 °C and with the maximum meaning 766 °C and 786 °C was due to the "cold" phases' crystallization - probably to the formation of diopside and olivine crystals. These two peaks show that the crystallization temperatures of these phases are shifted with respect to each other. The endothermic effect with a beginning/maximum of 1102/1171 °C is connected with the slag melting. During the cooling of the melted sample, the temperature of the crystallization is determined - it is 1159 °C. The practically complete amorphous state of the phases in the initial granulated slag confirms the relationship of the heat meanings of "cold"

crystallization (153 J/g), melting (152 J/g) and melt crystallization at cooling (154 J/g). According to the data obtained, the heating of high-magnesian glassy slag up to 1250 °C and its cooling at a rate of 20 °C/min lead to its transition from an amorphous state to a crystal state. The value of the stability factor of the glassy state of  $\Delta T$  for the investigated slag sample is equal to 98 °C, which points to the stability of the amorphous state.

The microstructure of the initial granulated slag is represented mainly by glass (Fig. 21). There are multiphase areas on the surface of the section and globular particles with a size of 5 - 15  $\mu\text{m}$  are concentrated in them. The representation of the section in the characteristic emission of elements is evidence of the fact that the main slag component consists of magnesium, silicon, iron, aluminium and calcium oxides. The other part is represented by small insular edged parts (10 - 20  $\mu\text{m}$ ) with a high iron, silicon and magnesium oxide content. The globular phases (less than 1% of the section area) consist of solid solutions of iron and nickel sulphides and their compounds. The results of the determination of the elements' composition of the parts of the granulated slag showed (Table 11) that the main part of it is represented by glass, containing up to 23.0% Fe, 20.0% Si, 6.3% Ca, 6.8% Mg and 2.7% Al. Another silicate phase with a high magnesium (14.0 - 23.0%), silicon (16.6 - 18.3%) and iron (18 - 30%) oxides content is in close agreement with the ferrous olivine.

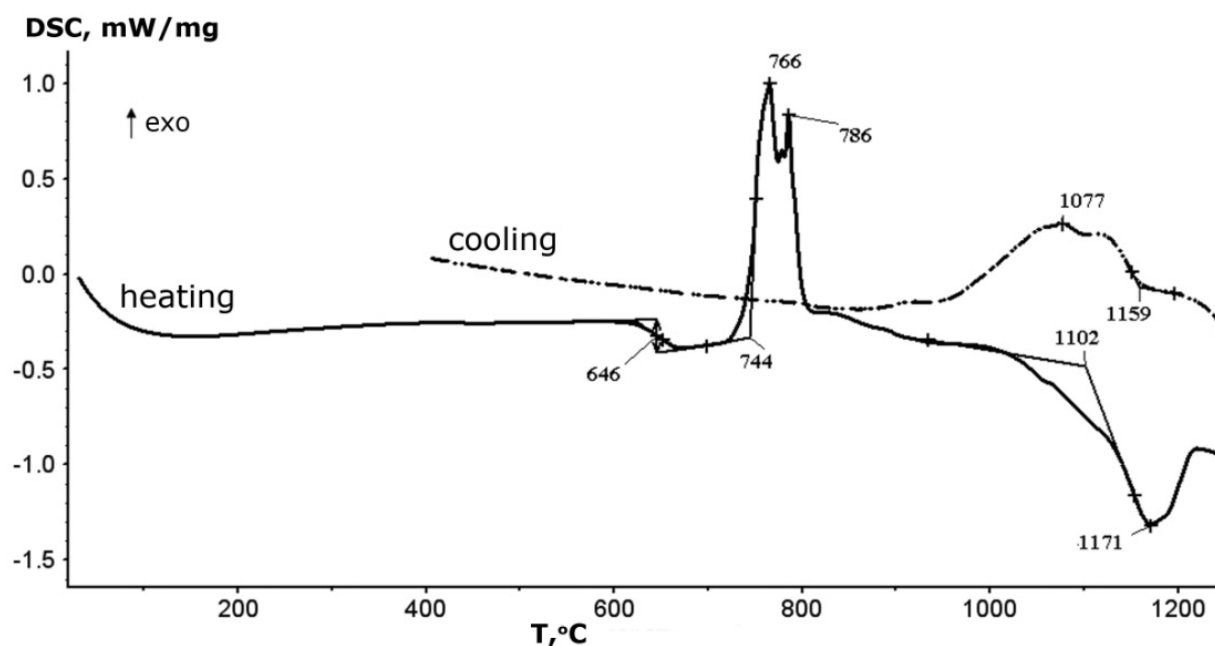


Fig. 20. DCK curves of granulated high-magnesian iron-silicate slag under heating and cooling at a rate of 20 °C/min

The nickel content in the glass is negligible (less than 0.1%), whereas its concentration in olivines reaches 0.2 - 1.2%. Sulphide metal shorts are either a mechanical suspension of matte or else are those solid solution phases which were isolated as the result of unbalanced slag cooling. The detailed analysis of the impurities' composition showed their heterogeneity. The grains consisting of the sulphide phases (27.8 - 29.1% S) concentrated in both nickel (up to 30.9%) and iron (up to 54.0%) are revealed in the impurities. The sulphide grain boundaries are metalized and the sulphur content in them is within the limits of 7.1 - 19.1%, Fe - 31.0 - 43.9%, Ni - 43.2 - 45.0% and Co - 1.6 - 2.6%.

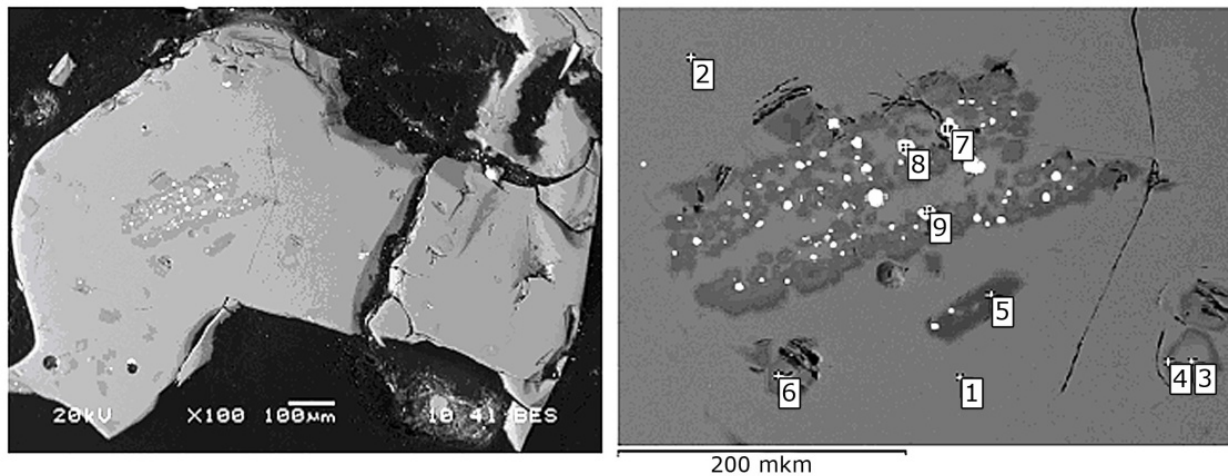


Fig. 21. Microstructure of the particle of high-magnesian iron-silicate granulated slag and EPMA points

The annealing at 1000 °C leads to the change of samples microstructure; the starting processes of solid crystallization can be seen in them, in contrast with the ferrous magnesian-free slags (Gulyaeva et al., 2011) where these phenomena proceed on the surface. The phases of the needle forms (Fig. 22) form in the heterogeneous part of the section - they have an average composition of  $(\text{Mg}_{0.79}\text{Fe}_{0.71}\text{Al}_{0.09}\text{Ca}_{0.16})\text{Si}_{1.10}\text{O}_4$ . Thus, the cut of olivine

№	Composition in the points of zonding	Content, %							
		Ni	Mg	Si	Al	Fe	S	Co	Ca
Before annealing (Fig. 21)									
1	$\text{Fe}(\text{Mg}_{0.67}\text{Ca}_{0.37})(\text{Si}_{1.74}\text{Al}_{0.24})\text{O}_6$	0	6.7	20.3	2.7	23.0	0.4	0.2	6.3
2	$\text{Fe}(\text{Mg}_{0.67}\text{Ca}_{0.37})(\text{Si}_{1.74}\text{Al}_{0.23})\text{O}_6$	0.1	6.8	20.1	2.6	22.3	0.4	0.2	6.1
3	$(\text{Mg}_{1.03}\text{Fe}_{0.97})\text{Si}_{1.05}\text{O}_4$	1.2	19.9	17.8	0.1	30.4	0	0.5	0.3
4	$(\text{Mg}_{1.40}\text{Fe}_{0.70})\text{Si}_{1.09}\text{O}_4$	0.4	14.0	16.6	0	22.9	0	0.2	0.5
5	$(\text{Mg}_{1.54}\text{Fe}_{0.53})\text{Si}_{1.07}\text{O}_4$	0.2	22.7	18.3	0	18.0	0	0.2	0.7
6	$(\text{Mg}_{1.20}\text{Fe}_{0.84})\text{Si}_{1.03}\text{O}_4$	0.5	17.1	17.1	0	26.3	0	0.4	0.4
7	Matte	16.8	0.2	0.4	0.1	51.0	26.8	1.4	0.1
8	Matte	21.3	0.2	0.4	0.1	47.0	26.2	1.5	0.2
9	Matte	33.0	0.2	0.4	0.1	38.2	24.7	1.3	0.2
After annealing (Fig. 22)									
10	$(\text{Mg}_{1.53}\text{Fe}_{0.52})\text{Si}_{1.05}\text{O}_4$	0.2	23.0	18.1	0.1	18.0	0	0.1	0.3
11	$(\text{Mg}_{1.46}\text{Fe}_{0.55})\text{Si}_{1.03}\text{O}_4$	0.2	22.1	17.8	0.1	18.9	0	0.2	0.6
12	$(\text{Mg}_{1.37}\text{Fe}_{0.67})\text{Si}_{1.05}\text{O}_4$	1.6	18.9	17.5	0.1	23.0	0	0.2	0.5
13	$(\text{Mg}_{1.15}\text{Ca}_{0.11}\text{Fe}_{0.64})\text{Si}_{1.07}\text{O}_4$	0.1	14.6	18.2	1.1	22.4	0.2	0.2	3.0
14	$\text{Fe}_{0.97}(\text{Mg}_{0.74}\text{Ca}_{0.49})(\text{Si}_{1.80}\text{Al}_{0.24})\text{O}_6$	0.1	7.2	20.2	2.7	21.3	0.4	0.2	7.8
15	Matte	23.3	0.2	0.4	0.1	40.7	31.1	1.2	0.2
16	$\text{Fe}_{0.75}\text{Ni}_{0.42}\text{S}(\text{Mg}_{1.42}\text{Fe}_{0.59})\text{Si}_{1.04}\text{O}_4$	0.3	21.0	17.7	0	20.2	0	0.1	0.8
17-20	$\text{Fe}_{0.94}(\text{Mg}_{0.74}\text{Ca}_{0.37})(\text{Si}_{1.75}\text{Al}_{0.24})\text{O}_6$	0.1	7.5	20.4	2.7	21.8	0.3	0	6.2
21-23	$\text{Fe}_{1.09}(\text{Mg}_{0.70}\text{Ca}_{0.39})(\text{Si}_{1.73}\text{Al}_{0.22})\text{O}_6$	0	6.7	19.6	2.5	24.5	0.5	0.1	6.3

Table 11. Elemental phase composition of the samples of granulated and annealed high-magnesian slags at EPMA points

crystals is shown clearly and their sizes increase to 60  $\mu\text{m}$ . The homogeneous glass breaks down into fine-dispersed (less than 0.5  $\mu\text{m}$ ) phases in which the  $\text{Fe}_{1.09}(\text{Mg}_{0.70}\text{Ca}_{0.39})(\text{Si}_{1.73}\text{Al}_{0.22})\text{O}_6$  composition differs slightly from the matrix, with a slight deviation in the iron (Table 11). The annealing also leads to changes in the microstructure of sulphide impurities, increasing their inhomogeneity. Fine-dispersed metallic phases containing 52.9 - 57.6% Ni, 36 - 38.9% Fe, 2.6 - 2.9% Co and 1.2 - 4.6% S also precipitate from an unbalanced matte and a monosulphide solid solution close in the composition to  $\text{Fe}_{1.03}\text{Ni}_{0.06}\text{S}$  forms.

Thus, the processes at the beginning of glass crystallization and the extraction of diopside and olivin are registered as a result of the annealing of the granulated slag of the shaft melting of oxide nickel ores. The main part of the nickel and cobalt is in a granulated slag as globules of a matte, while the sample annealing leads to the precipitation of fine-dispersed metallic phases enriched in nickel. Thermic effects conforming to devitrification processes, "cold" crystallization, melting and melting crystallization are determined and so they can be taken as basic effects for metallurgical calculation.

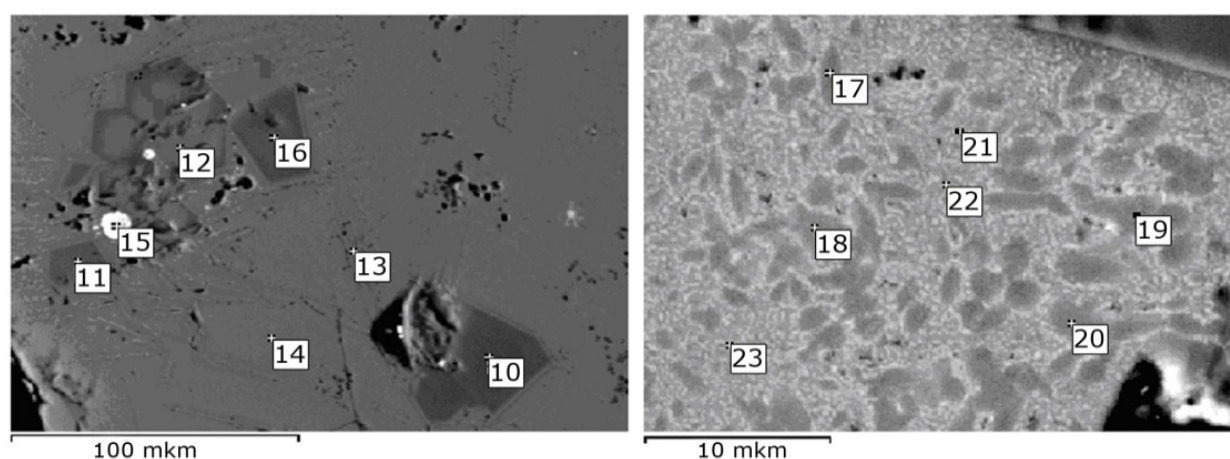


Fig. 22. Microstructure of particles of high-magnesian granulated slag after annealing at 1000 °C and EPMA points

## 7. Conclusion

The effect of melts' cooling rates on the phases' structure, composition and size, as well as the inter-phase distribution of impurity elements, have been estimated using exemplary slag samples taken from copper-zinc concentrates smelted in a Vanyukov furnace ("Sredneuralsky Copper Smelter Plant" JSC), combined smelting-converting ("Svyatogor" JSC), copper matte converting ("Sredneuralsky Copper Smelter Plant" JSC) and oxide ores smelting for matte ("Ufaleynickel" JSC). The cooling rate of iron oxide-sulphide melts affects the crystal structure, particle size and the number of forming phase. The cooling of the melt by using water granulation leads to the formation of glassy phases, the number of which increases with the content of  $\text{SiO}_2$ . The iron-silicate phases of variable composition, magnetite and sulphide components constitute the basis of the samples under study. Sulphides are represented by matte mechanical losses (particle size 50  $\mu\text{m}$ ) and fine inclusions (2-10  $\mu\text{m}$ ) formed from the melt during crystallization.

The amorphous constituent (glass) was observed in all the rapidly quenched samples. The devitrification temperature and the "cold" crystallization of the glassy phases of slags from the melting of copper-zinc concentrates and the converting of a copper matte are within the

range of 530-550 °C and 630 °C, respectively. The devitrification and cold crystallization of the granulated and high manganese slag processes from nickel production occur around temperatures of 650 to 740 °C.

The modes of the cooling of the melted slag determine the distribution of non-ferrous metals (copper, zinc, lead, nickel) between oxide and sulphide forms. The possibility of christophite Zn(Fe)S formation under rapid and slow slag cooling has been demonstrated for the first time. It was shown that the content of impurity elements in the phases arising depends upon the cooling rate and upon the Fe/SiO<sub>2</sub> ratio in these phases. The metal, copper-based, component accumulating antimony and arsenic was revealed in the slag sample taken from the copper matte conversion.

The forms of non-ferrous metals in the crystallized slag are able to be regulated by changing the Fe<sup>+3</sup>/Fe<sup>+2</sup> and CaO/SiO<sub>2</sub> ratios, the amounts of iron, CaO and MgO oxides. The data obtained is useful for the justification of processes for the re-extracting of precious metals.

## 8. References

- Biswas, K., Sontakke, A.D., Majumder, M. & Annapurna, K. (2010). Nonisothermal crystallization kinetics and microstructure evolution of calcium lanthanum metaborate glass. *J. Therm. Anal. Calorim*, Vol.101, pp. 143-151, ISSN 1388-6150.
- Cardona, N., Coursol, P., Vargas, J. & Parra, R. (2011). The Physical Chemistry of Copper Smelting Slags and Copper Losses at the Paipote Smelter. Part 2 - Characterization of industrial slags, *Canadian Metallurgical Quarterly*, Vol.50, No.4, pp. 330-340, ISSN 0008-4433.
- Dovchenko, V.A., Paretskii, V.M., Chakhotin, V.S. et al. (1997). Flotation Depletion of the Self-Decomposing Slags of the Slags of Melting of Copper Concentrates for Producing White Matte, *Tsvetn. Met.*, No.1, pp. 27-31, ISSN 0372-2929.
- Elliott, J. (1976). Phase relationships in the pyrometallurgy of copper. *Metallurgical Transactions*, Vol.7B, pp. 17-33, ISSN: 1073-5623.
- Gulyaeva, R.I., Selivanov, E.N. & Selmenskikh, N.I. (2011). Crystallization of oxide high iron melts. EPJ Web of Conferences, Vol.15, 01010. Published online 18.05.2011, available from <http://www.epj-conferences.org>.
- Karamanov, A. & Pelino, M. (2001). Vitrification of copper flotation waste. *J. Non-Crystalline Solids*, Vol.281, No.1-2, pp. 333-339, ISSN 0022-3093.
- Kopylov, N.I., Lata, V.A. & Toguzov, M.Z. (2001). *Interactions and Phase States in Molts Sulfides Systems*, ISBN 5-628-02752-9, Gilim, Almaty, in Russian.
- Koryukin, E.B., Litovskikh, S.N. & Kireeva, O.V. (2002). Flotation-Magnetic Scheme of Processing of Converter Slags. *Tsvetn. Met.*, No.8, pp. 18-20, ISSN 0372-2929.
- Mazurin, O.V. (1986). *Vitrification*, Nauka, Moscow, Russia.
- Mohapatra, B.K., Nayak, B.D. & Rao, G.V. (1994). Microstructure of and metal distribution in Indian copper converter slags – study by scanning-electron microscopy. *Mineral Processing and Extractive Metallurgy*, Vol.103, pp. C217-C220, ISSN 0371-9553.
- Moiseev, G.K. & Vyatkin, G.P. (1999). *Thermodynamic Simulation in Inorganic Systems*, YuUrGU, Chelyabinsk, Russia.
- Naboichenko, S.S., Nichiporenko, O.S., Murashev, I.B. et al. (1997). *Nonferrous Metal Powders*, Metallurgiya, Moscow, Russia.
- Nagamori, M. (1974). Metal loss to slag: Part I. Sulfidic and oxidic dissolution of copper in fayalite slag from low grade matte, *Metallurgical Transactions*, Vol.5, pp. 531-538. ISSN 1073-5623.

- Okunev, A.I. & Galimov, M.D. (1983). *Oxidation of iron and sulfur in the oxide-sulfide systems*, Nauka, Moscow, Russia.
- Roine, A. (2002). *Outokumpu HSC Chemistry for Windows*, (Outokumpu Research OY), Pori, www.outotec.com.
- Ruddle, R.W. (1953). *The Physical Chemistry of Copper Smelting*, Institution of mining and metallurgy, London.
- Rüffler, R. & Dávalos, J. (1998). Phase Analytical Studies of Industrial Copper Smelting slags: Part I: Silicate slags, *Hyperfine Interac.*, Vol.111, pp. 299–307, ISSN 0304-3843.
- Sarrafi, A., Rahmati, B., Hassani, H.R. & Shirazi, H.A. (2004). Recovery of Copper from Reverberatory Furnace Slag by Flotation. *Mineral Engineering*, Vol.17, No.3, pp. 457–459, ISSN 0892-6875.
- Selivanov, E.N., Okunev, A.I. & Moiseev, G.K. (2000). Phase Transformations during Cooling of the Slags of Melting of Copper Concentrates for Producing High-Grade Matte. *Rasplavy*, No.2, pp. 18–24, ISSN 0235-0106.
- Selivanov, E.N., Belyaev, V.V., Selmenskikh, N.I. & Pankratov, A.A. (2004). Forms of Metals in the Slag of Combined Melting–Converting of Copper Concentrates. *Rasplavy*, No.1, pp. 33–41, ISSN 0235-0106.
- Selivanov, E.N., Gulyaeva, R.I., Udoeva, L.Yu. et al. (2009a). Effect of the Cooling Rate on the Phase Composition and Structure of Copper Matte Converting Slags. *Russian Metallurgy (Metally)*, No.4, pp. 281–288, ISSN 0036-0295.
- Selivanov, E.N., Gulyaeva, R.I., Zelytin D.I. et al. (2009b). Effect of speed of cooling on structure of slag from of copper-zinc concentrates in Vanukov furnace. *Tsvetnyye Metally*, No.12, pp. 27-31, ISSN 0372-2929.
- Selivanov, E.N., Gulyaeva, R.I. & Selmenskich, N.I. (2010). Phase Formation in FeO<sub>x</sub>-SiO<sub>2</sub>-Cu<sub>2</sub>O-ZnO-FeS System during Melts Crystallization. *Defect and Diffusion Forum*, Vols. 297-301, pp. 602-607, ISSN 1662-9507.
- Sergeeva, S.V., Gulyaeva, R.I. & Selivanov, E.N. (2011). Features of crystallization of high-magnesian silicate slag. *13th Russian Conference on Composition and Properties of Melts of Metals and Slags*. Vol.3, pp. 99-102, Yekaterinburg, Russia, September 12-16, 2011.
- Spira, P. & Themelis, N.J. (1969). The Solubility of Copper in Slags. *Journal of Metals*, Vol.29, No.4, pp. 35-42, ISSN 0148-6608.
- Sycheva, G.A. & Polyakova, I.G. (2004). Nucleation of crystals in glasses based on blast furnace slag, *11th Russian Conference on Composition and Properties of Melts of Metals and Slags*. Vol.3, pp. 186-190, Yekaterinburg, Russia, September 14-16, 2004.
- Tokeda, Y., Ishiwata, S. & Yazawa, A. (1983). Distribution Equilibria of Minor Elements between Liquid Copper and Calcium Ferrite Slag. *Trans. Japan Inst. Metals*. Vol.24. No.10. pp. 518–528, ISSN 0021-4434.
- Vanyukov, A.V., Bystrov, V.P., Vaskevich, A.D. et al. (1988). *Melting in the Liquid Bath*, Metallurgiya, ISBN 5-229-00062-7, Moscow, Russia.
- Vanyukov, A.V. & Zaitsev, V.Ya. (1969). *Slags and Mattes of Nonferrous Metallurgy*, Metallurgiya, Moscow, Russia.
- Vanyukov, A.V. & Zaitsev, V.Ya. (1973). *Theory of Pyrometallurgical Processes*, Metallurgiya, Moscow, Russia.
- Vaysburd, S.E. (1996). *The Physical Chemistry Properties and Structural Features of Sulfide Melts*. Metallurgiya, ISBN 5-229-00903-9, Moscow, Russia.
- Yazawa, A. (1974). Thermodynamic considerations of copper smelting, *Canadian Metallurgical Quarterly*, Vol.13, No.3, pp. 443-455, ISSN 0008-4433.

© 2012 The Author(s). Licensee IntechOpen. This is an open access article distributed under the terms of the [Creative Commons Attribution 3.0 License](#), which permits unrestricted use, distribution, and reproduction in any medium, provided the original work is properly cited.

IntechOpen

IntechOpen